

1 acpd-15-24419-2015

2 A. Roth, J. Schneider, T. Klimach, S. Mertes, D. van Pinxteren, H. Herrmann, and S. Borrmann,
3 Aerosol properties, source identification, and cloud processing in orographic clouds measured by
4 single particle mass spectrometry on a Central European mountain site during HCCT-2010, Atmos.
5 Chem. Phys. Discuss., 15, 24419–24472, 2015

6

7

8 **Reply to Reviewer #1**

9

10 *Roth and co-authors describe a set of single particle mass spectrometer measurements of*
11 *ambient aerosol performed at a mountain site in Germany 2010. Ambient “out of cloud”*
12 *particles and cloud residuals were alternately analysed by bypassing or flowing air through a*
13 *counterflow virtual impactor, respectively. All data were combined and classified using a*
14 *series of approaches. Mass spectra were first clustered using c-means “fuzzy clustering” and*
15 *the resulting clusters were merged with similar types using distance metrics to create a more*
16 *manageable set of final particle classes. Differences between out of cloud particles and*
17 *cloud residuals were then assessed. Interstitial aerosol was not investigated. The main*
18 *findings are that cloud processed particles at the site are enriched in sulfate, nitrate and*
19 *ammonium ions relative to out of cloud particles. Larger, possibly aged, soot particles were also*
20 *found to represent a higher fraction of the in-cloud than out of cloud population, because of*
21 *internal mixing with hygroscopic inorganics. The manuscript is well written and scientifically*
22 *sound, with some nice tweaks on existing single particle mass spectral classification. I have*
23 *some minor comments only.*

24

25 We thank the reviewer for this positive rating of our manuscript.

26 In the following we answer the specific questions:

27

28 *The article would benefit from a map of the site and surrounding region/topography to*
29 *complement the local wind data. The proximity to local carbonaceous aerosol emission*
30 *sources could be included here. Also on this point, Figure 4 would be better represented in 2*
31 *panels. Readers will be more used to seeing a windrose like this applied to wind speed and*
32 *direction frequency. It is easy to miss that the radial axis is actually the fraction of the mass*
33 *spectral population detected. A standard windrose showing windspeed and direction would*
34 *be more useful. A second panel could show the dependence of particle hits on wind*
35 *direction. This could be normalised by frequency of wind from each sector if suitable.*

36

37 We added a map of the area to the supplement (Fig S1) and also a table with the population of
38 the cities in an area of approximately 50 km around the site (Table S1). We added a reference
39 to that Figure in section 2.1:

40 "A map of the surroundings of the measurement site along with a table giving the population
41 number of the cities within a radius of approximately 50 km around the site can be found in
42 the supplementary material (Figure S1 and Table S1)."

43

44 We replaced Figure 4 by three panels: One panel with a standard windrose showing
45 windspeed and direction frequency and two panels showing the number of analyzed particles
46 per wind direction, one of them normalized by the measuring time per wind direction.

47 In that context we also modified the description of Figure 4 in section 3.1.:

48 "Figure 4 shows the number of detected particles as a function of the local wind direction at
49 the Schmücke. Panel a) gives the standard wind rose for the whole time period. The
50 dominating wind direction was southwest, with about 50% probability for wind directions
51 between 200 and 270°. This direction corresponds to the requirements for cloud events. The
52 absolute number of detected particles is given in Panel b), showing that the majority of the
53 detected particles were measured when the wind came from southwest. However, as shown in
54 Panel c), per unit of time more particles were detected when the local wind direction was
55 between 0 and 90°. In these directions lie several larger cities (Erfurt, Weimar, Jena, see Map
56 in Figure S1) such that in general a higher pollution level may be expected."

57

58 *An expanded discussion of the merits of fuzzy clustering would be helpful. My understanding*
59 *is that the advantage is that each spectrum can "belong" to several clusters to differing*
60 *extents. However the classification approach here is exclusive, in that all spectra end up*
61 *"belonging" to only one cluster or group. In this case, what is the advantage over traditional*
62 *"hard" clustering techniques like neural network algorithms or k-means?*

63

64 In our case, we did not make a full use of the advantages that fuzzy clustering can give. This
65 would be a much more extended analysis. We chose the fuzzy means algorithm for two
66 reasons:

67 1) In tests that we performed with known data sets, consisting of a certain number of real
68 mass spectra from two particle types with the typical spectrum-to-spectrum variation,
69 it had turned out that with the fuzzy approach yielded a better result than the k-means
70 (Roth, 2014).

71 2) In our analysis, only those spectra were assigned to a cluster whose correlation
72 between the mass spectrum and the cluster center (after the termination threshold was
73 reached) was higher than 0.7. All other mass spectra (which had correlations smaller
74 than 0.7 with all clusters) were sorted into the "others" cluster. This "others" cluster
75 was then analyzed further by searching for certain marker peaks, as described in
76 section 2.4.4. This would not have been possible with the k-means algorithm, because
77 the k-means assigns all mass spectra to the "best" cluster, i.e. to that with the highest
78 correlation, even if the absolute correlation coefficient is small.

79

80 We added this explanation to section 2.4.1:

81 "The main reason for choosing the fuzzy c-means algorithm was that in a test with two
82 distinct particle types from laboratory data the fuzzy c-means yielded the best results (Roth,
83 2014). Furthermore, the fuzzy c-means accounts for mass spectra that don't fit to any cluster
84 by creating one additional group of spectra ("others"). These mass spectra can then be treated
85 separately by searching for certain marker peaks (see sections 2.4.3 and 2.4.4)."

86

87 *In section 2.4.2 it is not clear how the authors determined a false positive or false negative*
88 *assignment of a spectrum to an "incorrect" cluster. How is the incorrect assignment*
89 *identified? Hasn't the particle already been objectively assigned mathematically to the*
90 *most "correct" cluster using Pearson's r?*

91

92 From the mathematical point of view, the algorithm assigns each mass spectrum to the "best"
93 cluster, i.e. to that having the highest correlation to the mass spectrum in question. But
94 manual inspection of the mass spectra sometimes suggested that certain spectra belonged to
95 another particle type because of certain marker peaks. Although we compressed the peak
96 height (by a power of 0.5) it cannot be ruled out that single large peaks (especially K^+ or Na^+)
97 lead to a high correlation coefficient to a specific cluster, while smaller peaks, which can by

98 much more characteristic for a certain particle type, are not sufficiently considered by the
99 correlation.

100

101

102 *After the positive and negative mass spectra were normalised separately, they were*
103 *combined and normalised again. Why are they normalised again? Isn't this redundant? Or is*
104 *it simply to express everything as a fraction of 1 rather than 2?*

105

106 You are right, it is only done to express everything as a fraction of 1 for convenience.

107

108 *In section 2.4.3, last line, what are the counting statistics that the authors refer to?*

109

110 Counting statistics in this case refers to the counted number of particles of a certain type and
111 the assumption that the occurrence of these particles can be described by Poisson statistics.
112 Thus, the error bar for those particle types identified by the marker peak search is the square
113 root of the counted number of particles. We added this information to section 2.4.3.

114

115 *Section 3.2.4 contains only two sentences, but to me this is one of the most interesting*
116 *findings in the article. The possibility of catalytic oxidation of SO₂ (and other species like*
117 *DMS) in by iron and vanadium has impacts for the atmospheric lifetime and climate impacts*
118 *of thee particles. This is briefly referred towards the end of section 3.4 but the authors have*
119 *good evidence here and should expand the discussion to consider their results in the context*
120 *of other single particle studies that have focused on this topic, eg (Gaston et al., 2010; Ault et*
121 *al., 2010).*

122

123 Thank you for pointing this out. We added the following discussion on that issue to section
124 3.2:

125

126 "The presence of metals in cloud droplets has important implications for the oxidation of
127 sulphur containing species in the aqueous phase. Catalytic oxidation of SO₂ to sulphate by
128 transition metals as Fe and Mn (Calvert et al., 1985), but also Ti (Harris et al., 2013) and V
129 (Ault et al., 2010) is a process that has long been recognized (Calvert et al., 1985; Bradbury et
130 al., 1999), but data obtained during HCCT2010 have shown that this process is of higher
131 importance than previously thought (Harris et al., 2013). In marine environments, dimethyl
132 sulphide can be catalytically oxidized by vanadium to methanesulphonic acid (Gaston et al.,
133 2010). Enrichment of these transition metals in cloud droplets may be explained by cloud
134 processing: Transition metal-catalysed sulphate production in the cloud droplets leads to a
135 higher sulphate content of the metal-containing aerosol particles remaining after cloud
136 evaporation and thereby to a better activation of these particles in the next cloud formation
137 process."

138

139 *Section 3.2.3 The difference in hygroscopic behaviour for smaller soot particles with little*
140 *inorganic content and larger soot particles with higher inorganic content has been predicted*
141 *in Western Europe using single particle mass spectrometry previously and found to agree*
142 *well with HTDMA measurements (Healy et al., 2014).*

143

144 We included a reference to the findings of Healy et al. (2014) in section 3.2.3:

145 "Similar findings have been reported for growth factors of coated black carbon particles
146 measured in Paris using a hygroscopic tandem differential mobility analyser and a single
147 particle mass spectrometer (Healy et al., 2014b)."

148

149 *Page 24420, line 2: replace "have been" with "were"*

150

151 Changed

152

153 *24421, line 20: replace "during" with "within"*

154

155 We removed "during individual clouds" because it is not necessary here

156

157 *24422, lines19-21: Rephrase, unclear*

158

159 We changed the sentence to: "SO₂ oxidation in these clouds was inhibited by a lack of H₂O₂
160 and by the low pH-values, such that the observed sulphate in the cloud water derived most
161 likely from pre-existing aerosol."

162

163 *24423, line 16: replace "in southwesterly direction" with "facing southwest"*

164

165 Changed

166

167

168

169 **Reply toReviewer #2**

170 *This study presents the measurements from a field campaign where several on-line*
171 *instruments were operating side by side. The focus of this paper is to characterize the*
172 *chemical composition of aerosol particles measured by a single particle laser ablation*
173 *instrument and determine how different aerosol species are activated into cloud droplets.*
174 *Cloud droplet residues were analyzed using a counter flow virtual impactor (CVI). Aerosol*
175 *chemical composition and size distribution are provided by a single particle laser ablation*
176 *instrument (ALABAMA). This instrument is capable of generating both positive and negative*
177 *spectra from individual particles and therefore has the unique feature of providing information*
178 *of aerosol mixing state. Single particle spectra measured by the ALABAMA were classified*
179 *using fuzzy clustering. This paper is well written and organized and I recommend it for*
180 *publication. However, some additional information or discussion should be included.*

181

182 We thank the reviewer for this positive rating of our manuscript.

183 In the following we answer the specific questions:

184

185 *Was any attempt made to quantify the measurements from the ALABAMA using co-located*
186 *instrumentation? How did the size distribution measured by ALABAMA compare with that of*
187 *the OPC?*

188

189 The ALABAMA size distribution is not representative for the ambient size distribution. The
190 detection has its maximum between 550 and 600 nm, the ablation efficiency between 350 and
191 600 nm. The size distribution shown in Figure 3 can't be compared to the OPC size
192 distribution. Thus, we report only the relative abundance of particles. The total number of
193 particles detected by ALABAMA per time correlates rather well with the total number
194 concentration measured by the OPC ($r = 0.72$), such that we can assume a representative
195 sampling over the whole campaign time. But since the laser ablation method is not
196 quantitative by nature of the ablation and ionization process (as we stated in section 2.1) we
197 did not make any attempt to quantify the ALABAMA data.

198

199 *CVI inlets can often lead to enrichment of aerosol particles. Has this CVI been validated to*
200 *through comparisons with a whole air inlet (clouds particles +interstitial particles)/interstitial*
201 *inlet set up? This information is not included in Mertes et al., 2005. More information on the*
202 *flows and counter flows (and enrichment factors) of the CVI could be included in the*
203 *discussion.*

204

205 The enrichment factor of the CVI is given by the ratio of the air flow in the CVI wind-tunnel
206 to the sample flow inside the CVI inlet. Since both quantities are measured, the enrichment
207 factor can be calculated. Typical values are around 7 (ranging between 4.6 and 11.3). The
208 sampling efficiency of the CVI is determined by comparing the number of residuals counted
209 behind the CVI and the number of cloud droplets measured outside and by comparing the
210 LWC measured in the CVI sampling line and the LWC measured outside. Both the
211 enrichment factor and sampling efficiency were provided as a function of time and have been
212 applied to all quantitative instrumentation that was used in HCCT (for example the AMS,
213 Schneider et al., manuscript in preparation).

214 For the ALABAMA analysis, however, this enrichment and sampling efficiency correction is
215 not necessary, because we restrict the data evaluation and presentation to the relative
216 abundance of particles.

217
218

219 *Section 2.2: Can the authors provide more information on the types of clouds that were*
220 *studied, and how the out of cloud periods were chosen? How are these out of cloud periods*
221 *thought to be representative of aerosol particles activated into clouds, e.g include information*
222 *on air mass trajectories and on wind direction?*

223
224 Detailed information on the cloud type and meteorological conditions of each FCE is given in
225 the supplement to Tilgner et al (2014). We added brief information on the cloud conditions to
226 Table 1 and included a reference in section 2.2:

227 "Detailed information on cloud type and meteorological conditions of the individual FCEs is
228 given in the supplement to Tilgner et al. (2014)."

229 The out-of-cloud periods were treated in different ways: For Figure 6 all available data from
230 in-cloud and out-of-cloud were analyzed. This is described in section 3.2.

231 For the analysis presented in section 3.4, we selected air masses with comparable origins
232 based on HYSPLIT back trajectories for in-cloud and out-of-cloud conditions. As an
233 additional criterion it was required that the local wind direction at the Schmücke was
234 constant. This is described in section 3.4 and Table 5.

235

236 *The authors mention that after cloud processing, aerosol particles contain higher amounts of*
237 *nitrate and sulphate. They mention that the increases in nitrate and sulphate particles will*
238 *increase particle hygroscopicity and their ability to act as CCN. It is true that higher fractions*
239 *of inorganic ions will increase the hygroscopicity of the aerosol particle, however given the*
240 *size of the particles studied (> 200 nm) it is likely that they will be good CCN independent of*
241 *their aerosol composition.*

242

243 We agree, but there is no reason why the same cloud processing should not take place in all
244 cloud droplets, and thereby also in cloud droplets that were activated by smaller particles that
245 are just at the edge of the activation diameter. We added a statement to clarify this at the end
246 of section 3.4:

247 "This process will occur in all cloud droplets formed from all CCN sizes and therefore
248 influence also the CCN properties of aerosol particles smaller than analyzed here. For small
249 particles that are in the size range of the activation diameter for a specific supersaturation the
250 chemical composition plays an important role for the activation."

251

252 *For the mineral particles (Section 3.2.4) why do the authors think that there is such a*
253 *difference in activated aerosol composition? All particles of the sampled size should,*
254 *according to theory, be activated into clouds. Chemistry of aerosol particles is not thought to*
255 *play a role in the activation efficiency of aerosol particles with diameters > 200 nm (Duseck et*
256 *al., 2006)*

257

258 This effect may be due to metal-catalyzed sulfate formation in the cloud droplets. In the reply
259 to reviewer #1, we argued as follows:

260

261 "The presence of metals in cloud droplets has important implications for the oxidation of
262 sulphur containing species in the aqueous phase. Catalytic oxidation of SO₂ to sulphate by
263 transition metals as Fe and Mn (Calvert et al., 1985), but also Ti (Harris et al., 2013) and V
264 (Ault et al., 2010) is a process that has long been recognized (Calvert et al., 1985; Bradbury et
265 al., 1999), but data obtained during HCCT2010 have shown that this process is of higher
266 importance than previously thought (Harris et al., 2013). In marine environments, dimethyl
267 sulphide can be catalytically oxidized by vanadium to methanesulphonic acid (Gaston et al.,
268 2010). Enrichment of these transition metals in cloud droplets may be explained by cloud
269 processing: Transition metal-catalysed sulphate production in the cloud droplets leads to a
270 higher sulphate content of the metal-containing aerosol particles remaining after cloud
271 evaporation and thereby to a better activation of these particles in the next cloud formation
272 process."

273
274

275 Minor comments:

276 **Page 24420, Line 14** suggestion: "having a diurnal variation"

277

278 changed

279

280 **Page 24421, Line 1:** On one hand, the presence...

281

282 changed

283

284 **Line 28:** What is meant by individual cloud?

285

286 We deleted "during individual clouds" because it was not necessary. The sentence now reads:
287 "This technique has been coupled with on-line aerosol mass spectrometry before, such that the
288 composition of cloud droplets can be measured with high time resolution."

289

290 **Page 24422, Line 20:** The second part of this sentence needs to be rephrased.

291

292 We changed the sentence to: "SO₂ oxidation in these clouds was inhibited by a lack of H₂O₂
293 and by the low pH-values, such that the observed sulphate in the cloud water derived most
294 likely from pre-existing aerosol."

295

296 **Section 2: Experiments and data evaluation:** Although mentioned later on in the manuscript, it
297 would be useful to have information where the site is located with respect to the nearest city, Suhl in
298 the methods section.

299

300 We have included a map with the surrounding cities and a table with the population of these
301 cities in the supplementary material and added a sentence to the introduction:

302 "A map of the surroundings of the measurement site along with a table giving the population
303 number of the cities within a radius of approximately 50 km around the site can be found in
304 the supplementary material (Figure S1 and Table S1)."

305

306 **Page 24423, Line 24:** I assume that the interstitial aerosol was not detected because of their small
307 size. Can the authors include this information? Were any size distribution measurements made
308 between the interstitial inlet and the CVI to calculate aerosol activation profiles?

309

310 Yes, with the ALABAMA it was not possible to detect interstitial aerosol. Size distribution
311 measurements using SMPS have been made by TROPOS and will be published in a separate
312 paper.

313 We clarified the reasons for not measuring interstitial in section 2.1:

314 "We did not attempt to detect interstitial aerosol because the ALABAMA size range (starting
315 at 150 nm, see below) does not permit detection of small, unactivated particles."
316

317 **Page 24424, Line 20:** The authors mention that the HR-ToF-AMS and the MAAP were operating
318 continuously alongside the ALABAMA. Were the fractions of soot measured by the ALABAMA
319 comparable with the fractions of BC measured by the combined HR-ToF-AMS+MAAP.
320

321 The ALABAMA measures a number fraction of soot-containing particles in a size range
322 between 150 and 900 nm. All particle types contained also secondary inorganic material like
323 sulfate and nitrate (as stated in section 2.4.4). Thus the mass fraction of soot may be much
324 smaller than the number fraction of soot-containing particles.

325 Additionally, the size ranges are different: The MAAP has no size selective inlet, the AMS
326 inlet transmits between 60 and 700 nm. Thus, the number fraction measured by the
327 ALABAMA can hardly be compared to the mass fraction of soot inferred from AMS/MAAP
328 measurements. For completeness, we give here the mass fractions obtained from
329 AMS/MAAP (resp. PSAP) measurements:
330

	ALABAMA number fraction	AMS/MAAP/PSAP mass fraction	
331			
332	Out-of-cloud	13.6%	7.1%
333	Cloud residuals	27.0%	1.3%
334			

334

335

336 **Page 24425, Line 11:** It would be useful to provide a summary of the criteria described by Tilgner.

337

338 We added a brief explained how the full cloud events were inferred to section 2.2:

339

340 During the campaign a measurement period was considered as a “full cloud event” (FCE) if
341 the following criteria were fulfilled: liquid water content (LWC) of the summit site cloud
342 above 0.1 gm^{-3} , wind direction from the southwest ($200\text{--}250^\circ$ sector), wind speed at the
343 Schmücke site between 2 ms^{-1} and 12 ms^{-1} , no fog at the two valley sites, no precipitation at
344 any site, and air temperature above 0°C . In the course of the data analysis, only those FCEs
345 were chosen that fulfilled connected flow conditions which were inferred using cross-
346 correlations and coefficient of divergence (COD) for O_3 , particle number concentration in the
347 Aitken mode (49 nm) and in the accumulation mode (217 nm). For details see Tilgner et al.
348 (2014). Overall, 14 FCEs were identified and evaluated (Table 1).
349

350 **Line 16:** What is the number of spectra required for statistical evaluations?
351

351

352 Assuming Poisson statistics for the occurrence of a particle of a certain particle type, we
353 required to have at least 100 particles per event. This information is also given in the caption
354 of Figure 9 where the FCEs are individually analyzed.
355

356 **Page 24426, Line 20:** The abstract states that more than 170,000 bipolar mass spectra were obtained
357 while sampling out of cloud aerosol and more than 14,000 bipolar mass spectra were measured from
358 cloud residues.
359

359

360 The numbers on Page 24426 are correct. We changed the numbers in the abstract to "more
361 than 160 000" and "more then 13 000".

362

363 **Page 24427, Line 3:** Define MPIC and TROPOS.

364

365 Both acronyms occur only once in the manuscript, thus we decided not to use them anymore.

366

367 **Page 24429, line 22:** remove "actual"

368

369 done

370

371 **Page 24430, Line 2:** Reformulate sentence "Due to the fact that a reduced data set....."

372

373 We changed that sentence to: "This reduced test set contained no particles of the type
374 "mineral dust" and "Ca"."

375

376 **Page 24430, Line 27:** "more from fuel combustion than.."

377

378 No, this sentence is correct, because without the references it reads:

379 "...while Vanadium (V^+ , m/z 51) originates rather from fuel combustion and industrial
380 sources like refineries than from mineral dust."

381

382 **Figure 3:** Relative high fractions of soot particle were observed by the ALABAMA. How do these
383 compare to the fractions of soot observed by the MAAP + HR-ToF-AMS instrument? Was there any
384 attempt to compare absolute numbers/volume measured by the MAAP/HR-ToF-AMS with that of
385 ALABAMA.

386

387 See our reply to the same subject above.

388

389 **Page 24432, Line 9:** Laser ablation techniques have a tendency to be sensitive to matrix effects that
390 favor certain species with low ionization efficiencies, e.g. K. Do the authors consider that matrix
391 effects influence the measured composition of the aerosol particles?

392

393 This is certainly a general problem in the laser ablation technique and explains the high
394 relative abundance of the type "org, K" and "K". Also, detection of metals like Fe, V, and Ni
395 is likely to be favored by this technique. Thus, the number fraction observed by ALABAMA
396 may not reflect in absolute terms the number fraction in ambient air. However, these effects
397 are the same for all subsets of this study, such that the observed differences between the
398 individual cloud events and between the cloud residuals and the out-of-cloud aerosol are
399 meaningful.

400

401 **Page 24432, Line 14:** Aerosol particles with diameters between 200 nm and 450 nm are relatively
402 large. Freshly emitted (anthropogenic particles) or freshly formed aerosol particles are principally
403 measured at diameters < 100 nm.

404

405 We agree. These particles can't be "freshly" emitted. But since these particles are found in the
406 smaller size classes of the ALABAMA we suggest "recently" emitted and rephrased this
407 statement to: "This indicates that these particles were recently emitted and had only little time
408 to grow by condensation or coagulation."

409

410 **Page 24432, Line 15:** “had no time to grow by condensation...”

411

412 See above

413

414 **Page 24432, Line 26:** east north-east direction

415

416 According to the suggestion of Reviewer #1 we modified Figure 4 and thus changed the
417 paragraph describing Figure 4:

418 "Figure 4 shows the number of detected particles as a function of the local wind direction at
419 the Schmücke. Panel a) gives the standard wind rose for the whole time period. The
420 dominating wind direction was southwest, with about 50% probability for wind directions
421 between 200 and 270°. This direction corresponds to the requirements for cloud events. The
422 absolute number of detected particles is given in Panel b), showing that the majority of the
423 detected particles were measured when the wind came from southwest. However, as shown in
424 Panel c), per unit of time more particles were detected when the local wind direction was
425 between 0 and 90°. In these directions lie several larger cities (Erfurt, Weimar, Jena, see Map
426 in Figure S1) such that in general a higher pollution level may be expected."

427

428

429 **Page 24434:** The authors state that their measurements are different to those observed in other
430 studies with other instruments (Aerodyne, AMS). The reason for this is explained as being a result of
431 the short averaging time of the Aerodyne instrument compared with a single particle instrument.
432 Is there so much variation observed over the period of the cloud that would cause different
433 averaging results? Are the size distributions measured by the two instruments in the two studies
434 comparable? It would be better for the authors to focus on the comparison with Schneider et al.,
435 from the same study than from observations by Drewnick et al. (2005). In general how does the
436 fraction of organic material observed by ALABAMA compare with that observed by the C-ToF-AMS
437 instrument. How does the size distribution of aerosol particles measured by the ALABAMA compare
438 with that measured by the C-ToF-AMS instrument?

439 How much was the scavenging efficiency of organic species dependent on their mixing state?

440

441 As explained earlier, the size distribution of the ALABAMA is not quantitative and can
442 therefore not be compared with the size distribution measured by the AMS. Also a
443 comparison of the organic mass fraction measured by the AMS with the number fraction of
444 ALABAMA is problematic, because:

- 445 - We would compare number fraction and mass fraction
- 446 - The single particle types containing organic material ("org, K", "org", "amines",
447 "diesel exhaust", "biomass burning") contain also other material (like nitrate and
448 sulfate) that would not be accounted for. In the AMS data product, these mixed
449 particles would be separated into organic and inorganic mass. On the other hand, the
450 AMS would not detect refractory material in biomass burning aerosol.

451

452 Thus, we conclude that such a comparison would be misleading and would be subject of a
453 much more detailed analysis, including a discussion of the measuring capabilities of both
454 instruments. This would clearly be beyond the scope of this paper.

455

456

457 **Page 24434, Line 10:** “data” “single particle analysis”.

458

459 changed

460
461 Page 24435, Line 4: "...mass spectra show peaks"
462
463 changed
464
465 **Page 24435, Line 9:** the definition of TMA should be made earlier.
466
467 We defined TMA on its first occurrence.
468
469 **Figure 8:** The AMS biomass burning axis could be change to be in the same range as the EBC axis
470 That would lead to a too small signal in the graph. In contrast, we preferred to expand the axis
471 (0 to 0.4 $\mu\text{g m}^{-3}$) such that the correlation of the AMS biomass burning signal and the EBC
472 signal is better visible.

473

474

475

476 **References**

477

478

- 479 Ault, A. P., Gaston, C. J., Wang, Y., Dominguez, G., Thiemens, M. H., and Prather, K. A.:
480 Characterization of the Single Particle Mixing State of Individual Ship Plume Events
481 Measured at the Port of Los Angeles, *Environ. Sci. Technol.*, 44, 1954-1961,
482 10.1021/es902985h, 2010.
- 483 Bradbury, C., Bower, K. N., Choularton, T. W., Swietlicki, E., Birmili, W., Wiedensohler, A.,
484 Yuskiewicz, B., Berner, A., Dusek, U., Dore, C., and McFadyen, G. G.: Modelling of
485 aerosol modification resulting from passage through a hill cap cloud, *Atmos. Res.*, 50,
486 185-204, [http://dx.doi.org/10.1016/S0169-8095\(98\)00104-5](http://dx.doi.org/10.1016/S0169-8095(98)00104-5), 1999.
- 487 Calvert, J. G., Lazrus, A., Kok, G. L., Heikes, B. G., Walega, J. G., Lind, J., and Cantrell, C.
488 A.: Chemical mechanisms of acid generation in the troposphere, *Nature*, 317, 27-35,
489 10.1038/317027a0, 1985.
- 490 Gaston, C. J., Pratt, K. A., Qin, X., and Prather, K. A.: Real-Time Detection and Mixing State
491 of Methanesulfonate in Single Particles at an Inland Urban Location during a
492 Phytoplankton Bloom, *Environ. Sci. Technol.*, 44, 1566-1572, 10.1021/es902069d,
493 2010.
- 494 Harris, E., Sinha, B., van Pinxteren, D., Tilgner, A., Fomba, K. W., Schneider, J., Roth, A.,
495 Gnauk, T., Fahlbusch, B., Mertes, S., Lee, T., Collett, J., Foley, S., Borrmann, S.,
496 Hoppe, P., and Herrmann, H.: Enhanced Role of Transition Metal Ion Catalysis
497 During In-Cloud Oxidation of SO₂, *Science*, 340, 727-730, 10.1126/science.1230911,
498 2013.
- 499 Healy, R. M., Evans, G. J., Murphy, M., Jurányi, Z., Tritscher, T., Laborde, M., Weingartner,
500 E., Gysel, M., Poulain, L., Kamilli, K. A., Wiedensohler, A., O'Connor, I. P.,
501 McGillicuddy, E., Sodeau, J. R., and Wenger, J. C.: Predicting hygroscopic growth

502 using single particle chemical composition estimates, Journal of Geophysical
503 Research: Atmospheres, 119, 9567-9577, 10.1002/2014JD021888, 2014.
504 Roth, A.: Untersuchungen von Aerosolpartikeln und Wolkenresidualpartikeln mittels
505 Einzelpartikel-Massenspektrometrie und optischen Methoden, PhD Thesis (in
506 German), University Mainz, 178 pp., <http://d-nb.info/1053202164/34>, 2014.
507 Tilgner, A., Schöne, L., Bräuer, P., van Pinxteren, D., Hoffmann, E., Spindler, G., Styler, S.
508 A., Mertes, S., Birmili, W., Otto, R., Merkel, M., Weinhold, K., Wiedensohler, A.,
509 Deneke, H., Schrödner, R., Wolke, R., Schneider, J., Haunold, W., Engel, A., Wéber,
510 A., and Herrmann, H.: Comprehensive assessment of meteorological conditions and
511 airflow connectivity during HCCT-2010, Atmos. Chem. Phys., 14, 9105-9128,
512 10.5194/acp-14-9105-2014, 2014.

513

514

515 **Aerosol properties, source identification, and cloud**
516 **processing in orographic clouds measured by single**
517 **particle mass spectrometry on a Central European**
518 **mountain site during HCCT-2010**

519

520 **A. Roth¹, J. Schneider¹, T. Klimach¹, S. Mertes², D. van Pinxteren², H.**
521 **Herrmann², and S. Borrmann^{1,3}**

522 [1] Particle Chemistry Department, Max Planck Institute for Chemistry, Hahn-Meitner-Weg
523 1, 55128 Mainz, Germany

524 [2] Leibniz Institute for Tropospheric Research (~~TROPOS~~), 04318 Leipzig, Germany

525 [3] Institute for Physics of the Atmosphere, Johann-Joachim-Becherweg 21, University of
526 Mainz, 55128 Mainz, Germany

527 Correspondence to: J. Schneider (johannes.schneider@mpic.de)

528

529

530 **Abstract**

531 Cloud residues and out-of-cloud aerosol particles with diameters between 150 and 900 nm
532 ~~have been~~were analysed by on-line single particle aerosol mass spectrometry during the six-
533 week study HCCT-2010 in September/October 2010. The measurement location was the
534 mountain Schmücke (937 m a.s.l.) in Central Germany. More than ~~1670~~-000 bipolar mass
535 spectra from out-of-cloud aerosol particles and more than ~~134~~-000 bipolar mass spectra from
536 cloud residual particles were obtained and were classified using a fuzzy c-means clustering
537 algorithm. Analysis of the uncertainty of the sorting algorithm was conducted on a subset of
538 the data by comparing the clustering output with particle-by-particle inspection and
539 classification by the operator. This analysis yielded a false classification probability between
540 13% and 48%. Additionally, particle types were identified by specific marker ions.

541 The results from the ambient aerosol analysis show that 63% of the analysed particles belong
542 to clusters ~~having~~indicating a diurnal variation, suggesting that local or regional sources
543 dominate the aerosol, especially for particles containing soot and biomass burning particles.

544 In the cloud residues the relative percentage of large soot-containing particles and particles
545 containing amines was found to be increased compared to the out-of-cloud aerosol, while in
546 general organic particles were less abundant in the cloud residues. In the case of amines this
547 can be explained by the high solubility of the amines, while the large soot-containing particles
548 were found to be internally mixed with inorganics, which explains their activation as cloud
549 condensation nuclei. Furthermore, the results show that during cloud processing, both
550 sulphate and nitrate are added to the residual particles, thereby changing the mixing state and
551 increasing the fraction of particles with nitrate and/or sulphate. This is expected to lead to
552 higher hygroscopicity after cloud evaporation, and therefore to an increase of the particles'
553 ability to act as cloud condensation nuclei after their cloud passage.

554

555 **1. Introduction**

556 | The interaction of aerosol particles and cloud droplets has several aspects: On ~~the~~ one hand,
557 the presence of a cloud condensation nucleus (CCN) is an essential prerequisite for the
558 formation of a cloud droplet, and the size and chemical composition of the aerosol particle
559 determines whether a particle acts at a certain temperature and supersaturation as a CCN or
560 not (e.g., Dusek et al., 2006b; Gunthe et al., 2009). On the other hand, cloud processing alters
561 the chemical composition of the cloud droplet such that after evaporation of the cloud droplet
562 the remaining aerosol particle is of different composition than the original CCN. The uptake
563 of nitric acid in the aqueous phase of cloud droplets has been observed (Hayden et al., 2008),
564 but also sulphate is known to be produced by oxidation of SO₂ in the cloud phase, either by
565 reaction with O₃ (Bower et al., 1991), H₂O₂ (Bower et al., 1997; Laj et al., 1997a) or by
566 transition metal induced oxidation (Harris et al., 2014). Both effects lead to a higher content
567 of water soluble inorganic material in the aerosol which is expected to enhance the cloud
568 formation potential of the particles.

569 Cloud particle sampling and separation from the not activated interstitial aerosol can be
570 achieved by applying a counterflow virtual impactor (CVI, Ogren et al., 1985; Mertes et al.,
571 2005b; Wendisch and Brenguier, 2013). This technique has been coupled with on-line aerosol
572 | mass spectrometry before, such that the composition of ~~the~~ cloud droplets ~~residues~~ ~~during~~
573 ~~individual clouds~~ can be measured with high time resolution (Drewnick et al., 2007; Allan et
574 al., 2008; Hayden et al., 2008) . The use of single particle mass spectrometry for single cloud
575 residual particle analysis (e.g., Gieray et al., 1997; Kamphus et al., 2010; Pratt et al., 2010;

576 Zelenyuk et al., 2010), gives not only the composition of the bulk residues but also the mixing
577 state of the cloud residues. Comparison with the aerosol observed shortly before cloud
578 formation can give information on the possible addition of chemical compounds in the cloud
579 phase and thereby evidence for cloud processing.

580 Several previous hill cap cloud experiments - considering the clouds as "stationary flow
581 processors" - have been conducted and results have been reported in the literature. One of
582 these is the FEBUKO experiment (Herrmann et al., 2005) which took place at the same field
583 site as the HCCT-2010 experiment reported here. The results from FEBUKO have shown a
584 measurable increase of sulphate and ammonium, but only in 2 of 3 investigated cases, and
585 only in the smallest particle size range (up to 140 nm; Brüggemann et al., 2005). The mass
586 production in the clouds was about 5% of upwind aerosol mass (in a size range between 60
587 and 300 nm, Mertes et al., 2005a). Tilgner et al. (2005) found from model calculations for the
588 same experiment that the mass increase is mainly due to HNO₃ uptake and only to a lesser
589 degree due to SO₂ oxidation.

590 The Kleiner Feldberg Cloud Experiment (Fuzzi et al., 1994; Wobrock et al., 1994) was
591 conducted in 1990. Off-line single particle analyses of cloud residues sampled via a
592 counterflow virtual impactor during this experiment are reported by Hallberg et al. (1994). It
593 could be shown that the majority of cloud residues contained soluble compounds whereas
594 insoluble particles remained in the interstitial air. Fuzzi et al. (1994) report from the Feldberg
595 Cloud Experiment that a general lack of gaseous NH₃ was observed in the cloud systems.
596 ~~Thus, the~~So clouds were acidic either by uptake of HNO₃ or by oxidation of NO₂ via O₃ in the
597 aqueous phase. SO₂ oxidation in these clouds was inhibited by a lack of H₂O₂ and by the low
598 pH-values, such that the observed sulphate in the cloud water derived most likely from pre-
599 existing aerosol. being not an explanation for the verified sulphate concentration in the cloud
600 water.

601 During the Great Dun Fell experiment which took place in 1993 an increased sulphate
602 concentration of the aerosol was observed after cloud passing (Laj et al., 1997b). Thereby also
603 the ammonium concentration increased based on the neutralization reaction with ammonia.
604 The increased sulphate concentration could be attributed mainly to SO₂ oxidation by H₂O₂ in
605 the cloud water and to a lesser extent by O₃ (Bower et al., 1997; Laj et al., 1997a).
606 Furthermore, even though the concentrations of iron and copper were low, an influence of

607 these elements on formation and depletion of photo-oxidants could be recognized (Sedlak et
608 al., 1997).

609 Here we report the results obtained from individual particle chemical analysis by on-line
610 single particle laser ablation mass spectrometry during the hill cloud experiment HCCT-2010,
611 which was conducted on the mountain site Schmücke in September and October 2010 in
612 Central Germany. The analysis includes cloud residual particles that were sampled from the
613 cloud using a CVI and aerosol particles that were measured during cloud-free periods.

614

615 **2. Experiments and data evaluation procedures**

616 **2.1. Measurement site and instrumentation**

617 The Hill Cap Cloud Thuringia (HCCT) 2010 experiment took place between 13 September
618 2010 and 25 October 2010, at the mountain ridge "Thüringer Wald" in Central Germany. The
619 same measurement sites were used as during two previous experiments (FEBUKO 2001 and
620 2002, Herrmann et al., 2005): (1.) an upwind site (Goldlauter, 605 m a.s.l., 10°45'20" E,
621 50°38'28" N), (2.) a summit site (Schmücke, 937 m a.s.l., 10°46'15" E, 50°39'19" N), and (3.)
622 a downwind site (Gehlberg, 732 m a.s.l., 10°47'32" E, 50°40'21" N). A map of the
623 surroundings of the measurement site along with a table giving the population number of the
624 cities within a radius of approximately 50 km around the site can be found in the
625 supplementary material (Figure S1 and Table S1). At the summit site Schmücke, two particle
626 inlets were installed ~~facing south-west in south-westerly direction~~ in separate windows at the
627 height of 15 m of a 3-story building that hosts a field station of the German Environmental
628 Protection Agency (*Umweltbundesamt*). The aerosol inlet was used to sample aerosol
629 particles with aerodynamic diameters (d_{aero}) smaller than 5 μm under cloud free conditions.
630 During cloudy periods the CVI (Mertes et al., 2005b) was additionally deployed to sample
631 cloud droplets with diameters larger than 5 μm . The single particle aerosol mass spectrometer
632 ALABAMA (Aircraft-based Laser Ablation Aerosol Mass Spectrometer) was operated while
633 manually alternating between these two inlets. We did not attempt to detect interstitial aerosol
634 because the ALABAMA size range (starting at 150 nm, see below) does not permit detection
635 of small, unactivated particles~~Interstitial aerosol was not detected by the ALABAMA and is~~
636 ~~therefore not considered in this study.~~

637 A detailed description of the mass spectrometer ALABAMA can be found in Brands et al.
638 | (2011). The particles enter the vacuum chamber via a Liu-type aerodynamic lens (Liu et al.,
639 1995a, b) and are focused to a narrow particle beam. Due to the pressure drop the particles are
640 accelerated when exiting the aerodynamic lens. The final particle velocity depends on their
641 size, shape and density. The particles are detected by the scattered light of two orthogonal
642 continuous wave Nd:VO₄ laser beams ($\lambda = 532$ nm). The optical detection of the particles
643 limits the particle size range for smaller particles to about 150 - 200 nm. The particle size
644 given as the vacuum aerodynamic diameter (d_{va}) can be derived from the time difference
645 between the two scattering signals by means of calibration with particles of known size. In
646 addition the time difference is used to calculate the time at which a particle will arrive at the
647 ionization region of the mass spectrometer. There the particle is evaporated and ionized in one
648 step by laser ablation with a pulsed Nd:YAG laser ($\lambda = 266$ nm). The resulting positive and
649 negative ions are detected by a bipolar time-of-flight mass spectrometer. The laser ablation
650 method is a qualitative method, such that it is not possible to relate the peak height to a mass
651 concentration of a certain compound (e.g., Middlebrook et al., 2003).

652 Figure 1 shows the measurement set-up and additionally operated instruments at the summit
653 site Schmücke. Besides the ALABAMA, an optical particle counter (OPC, Grimm, model
654 1.109, time resolution 6 s) as well as an Compact Time-of-Flight Aerosol Mass Spectrometer
655 (C-ToF-AMS, Aerodyne Research Inc., Drewnick et al., 2005) were run simultaneously.
656 Furthermore a High Resolution Time-of-Flight AMS (HR-ToF-AMS, Aerodyne Research
657 Inc., DeCarlo et al., 2006) and a multi-angle absorption photometer (MAAP, Thermo
658 Scientific, model 5012, time resolution 1 min) were operated continuously at the aerosol inlet.
659 The MAAP determines the mass concentration of equivalent black carbon (EBC, Petzold et
660 al., 2013) based on the absorption of particles sampled on a filter. The results from the C-
661 ToF-AMS and HR-ToF-AMS measurements are presented in an accompanying paper
662 (Schneider et al., 2015). Outside of the building, a particle volume monitor (PVM, Gerber
663 Scientific Inc., model 100, time resolution 1 min) for investigation of the liquid water content
664 (LWC) and a weather station (Davis Vantage Pro) for meteorological parameters were
665 installed. Additionally, Caltech active strand cloud water collectors (one stage, three stage,
666 and five stage) were mounted. The pH-value as well as the content of organic compounds of
667 | cloud water were analysed by off-line methods at [the Leibniz Institute for Tropospheric](#)
668 | [Research TROPOS](#). Furthermore, aliphatic amines were analysed from filtrated cloud water
669 samples (0.45 μ m syringe filters, Acrodisc 13, Pall, Dreieich, Germany) using an

670 ion chromatography method adopted from Facchini et al. (2008). Details of the method are
671 given elsewhere (van Pinxteren et al., 2015).

672

673 **2.2. Definition of Full Cloud Events (FCE)**

674 ~~During the campaign a measurement period was considered as a "full cloud event" (FCE)~~
675 ~~when the air masses passed all three measurement sites and when the criteria described in~~
676 ~~Tilgner et al. (2014) were fulfilled.~~ During the campaign a measurement period was
677 considered as a "full cloud event" (FCE) if the following criteria were fulfilled: liquid water
678 content (LWC) of the summit site cloud above 0.1 gm^{-3} , wind direction from the southwest
679 ($200\text{--}250^\circ$ sector), wind speed at the Schmücke site between 2 ms^{-1} and 12 ms^{-1} , no fog at the
680 two valley sites, no precipitation at any site, and air temperature above 0°C . In the course of
681 the data analysis, only those FCEs were chosen that fulfilled connected flow conditions which
682 were inferred using cross-correlations and coefficient of divergence (COD) for O_3 , particle
683 number concentration in the Aitken mode (49 nm) and in the accumulation mode (217 nm).
684 For details see Tilgner et al. (2014). ~~Overall~~ During HCCT-2010, 14 FCEs were identified
685 ~~((Tilgner et al., 2014)~~ and evaluated (Table 1). In this study we present the data from all cloud
686 residue measurements behind the CVI, but additionally the official FCEs are analysed
687 separately, thereby facilitating comparison with other data from HCCT-2010. FCEs showing
688 insufficient number of mass spectra for statistical evaluations (FCE2.1, FCE4.1, FCE5.1 and
689 FCE 26.2) are not considered in the following data analysis. Detailed information on cloud
690 type and meteorological conditions of the individual FCEs can be found in the supplement to
691 Tilgner et al. (2014), a brief description of the cloud conditions is included in Table 1.

692

693 **2.3. Back trajectory calculation**

694 Back trajectories for the air masses encountered during HCCT-2010 were calculated using
695 HYSPLIT (Hybrid Single-Particle Lagrangian Integrated Trajectory, Draxler and Rolph
696 (2012)). The air mass origin was determined 96 h before arriving at Mt. Schmücke with a
697 time resolution of 1 h. The coordinates of the Schmücke at a height of 500 m above the
698 ground were used as endpoint in the model. 500 m were chosen because the model orography
699 can't resolve a small scale mountain range like the Thüringer Wald with sufficient detail. The

700 back trajectories for the whole HCCT-2010 campaign can be found in the supplement (Figure
701 | [S1S2](#)). Back trajectories for the FCE are discussed in section 3.3.

702

703 **2.4. Analysis of single particle mass spectra**

704 During the whole HCCT-2010 campaign the ALABAMA sampled over 286 000 single
705 particle mass spectra. The mass spectra were distinguished between out-of-cloud aerosol and
706 cloud residual particles according to the inlets and the LWC. For the analysis of out-of-cloud
707 aerosol only measurement periods with an LWC < 0.05 g m⁻³ were considered (402 h) while
708 data sampled behind the CVI were only examined for an LWC > 0.1 g m⁻³ (228 h, 106 h
709 during FCEs). Upon inspection of the data set, a certain number of mass spectra were found to
710 contain ions of only one polarity. The appearance of such mono polar mass spectra was also
711 observed in other single particle mass spectrometer measurements (Bein et al., 2005;
712 Sodeman et al., 2005; Shields et al., 2007; Pratt et al., 2010) resulting either from technical
713 issues (e.g. tuning of high voltages) or from ion formation of only one polarity (Sodeman et
714 al., 2005). Negative ion mass spectra provide better information on secondary organic and
715 inorganic compounds (nitrate and sulphate) and thereby also on the mixing state of the
716 particles. However, in order to constrain the analysis to a consistent data set, monopolar mass
717 spectra were excluded and only mass spectra of both polarities were considered for the data
718 analysis presented here. Out of the remaining 177 752 bipolar single particle mass spectra
719 164 595 were obtained while sampling out-of-cloud aerosol and 13 157 while sampling cloud
720 residues (out of these 4 400 were obtained during FCEs).

721 **2.4.1. Clustering by fuzzy c-means algorithm**

722 The analysis method that is widely used and has become a standard method for single particle
723 mass spectra data is the clustering of the data set by similarities of the mass spectra (e.g., Hinz
724 et al., 1999; Silva and Prather, 2000; Murphy et al., 2003; Hinz et al., 2006; Zelenyuk et al.,
725 2006; Hinz and Spengler, 2007; Zelenyuk et al., 2008; Zhao et al., 2008; Dall'Osto et al.,
726 2009). The analysis presented here was conducted using the software tool CRISP (version
727 | 1.127, 64 bit) that was recently developed at [the Max Planck Institute for Chemistry MPIC](#)
728 (Klimach, 2012). It is based on the programming software IGOR Pro (version 6.3,
729 WaveMetrics). CRISP facilitates processing and management of large data sets. Data

730 processing includes mass calibration of the time-of-flight spectra, peak area integration, and
731 either automated clustering by one of the implemented algorithms (k-means or fuzzy c-
732 means), or manual clustering by inspection of every mass spectrum. Furthermore particle
733 spectra can be selected by specified criteria or according to additional external data sets. Here
734 the clustering was done using the fuzzy c-means algorithm (Bezdek, 1981; Bezdek et al.,
735 1984; Hinz et al., 1999). The main reason for choosing the fuzzy c-means algorithm was that
736 in a test with two distinct particle types from laboratory data the fuzzy c-means yielded the
737 best results (Roth, 2014). Furthermore, the fuzzy c-means accounts for mass spectra that don't
738 fit to any cluster by creating one additional group of spectra ("others"). These mass spectra
739 can then be treated separately by searching for certain marker peaks (see sections 2.4.3 and
740 2.4.4). All 177 752 bipolar mass spectra were first pre-processed separately by calculating the
741 square root of the peak intensity for every peak in order to reduce peak intensity differences.
742 Afterwards the mass spectra were normalized (positive and negative polarities separately) to
743 the sum of the peak intensities. After concatenation of both polarities the entire mass
744 spectrum was normalized again. In the algorithm the starting reference mass spectra for the
745 clustering are chosen as follows: The first mass spectrum of the data set is chosen as the first
746 reference. Hereupon the distance between the first reference and all further mass spectra is
747 calculated sequentially. If the Pearson correlation coefficient between the reference and the
748 actual mass spectrum is smaller than a threshold (chosen here: 0.8), the latter is regarded as
749 being significantly different from the first reference spectrum and is added as a further start
750 cluster reference. This procedure is repeated until the desired number of start clusters (here:
751 200) is obtained. The membership coefficient m_{ik} for every particle spectrum i to a cluster
752 reference k is calculated by:

$$753 \quad m_{ik} = \frac{1}{\sum_{j=1}^c \left(\frac{d_{ik}}{d_{ij}}\right)^{\frac{2}{f-1}}} \quad (1)$$

754 with the number of clusters c , the "fuzzifier" f and the distance d_{ij} between mass spectrum i
755 and reference j . The sum of all membership coefficients equals 1. The fuzzifier ($1 \leq f \leq \infty$,
756 originally introduced as "weighting exponent" by Bezdek (1981)) represents the fuzziness
757 (blurring, defocusing) of the classification. The fuzzifier value of 1.7 applied here was chosen
758 empirically on the basis of test data sets with known particle types and particle numbers. The
759 distance d_{ij} is calculated here based on the Pearson correlation coefficient r_{ij} ($0 \leq r_{ij} \leq 1$)
760 between the particle spectrum i and the cluster reference j via:

761 $d_{ij} = 1 - r_{ij}$ (2).

762 Every mass spectrum is compared to the start clusters, calculating correlation coefficient,
763 distance and membership coefficient. Afterwards a mean mass spectrum of every cluster is
764 calculated under consideration of the membership coefficients. The new mean cluster
765 spectrum serves as reference for the following run. Again correlation, distance and
766 memberships are calculated for every mass spectrum to the new cluster references. This
767 procedure is repeated until the membership difference of two consecutive iterations is smaller
768 than a termination threshold (here: 10^{-4}). Now every mass spectrum is assigned to that cluster
769 for which the Pearson correlation coefficient r_{ij} is highest, but only if r_{ij} is larger than a certain
770 threshold (here: 0.7). Mass spectra showing smaller correlation coefficients than this
771 threshold are sorted out and assigned to an additional cluster ("others").

772 The clustering of the current data set resulted in 159 clusters. This number is smaller than the
773 starting value of 200 clusters, confirming that the chosen number of 200 starting cluster was
774 large enough and that no particle types that significantly differ from the others were missed
775 by the algorithm. About 9% of all mass spectra were sorted out being represented by the
776 fraction "others". According to the fragmentation pattern considering characteristic peaks for
777 certain particle types, their combination (e.g. Hinz et al., 1999; Trimborn et al., 2002; Vogt et
778 al., 2003; Dall'Osto and Harrison, 2006; Pratt and Prather, 2010; Corbin et al., 2012) and
779 relative peak intensities, every cluster was assigned manually to a certain particle type.
780 Afterwards the number of obtained clusters was reduced by combining clusters of the same
781 particle type, if two mean cluster spectra j and k showed a Pearson correlation coefficient r_{jk}
782 larger than 0.7. In this way 65 cluster types remained which were further grouped into 19
783 different fragmentation types (plus "others") representing 11 distinguished particle types (plus
784 "others"), according to the criteria given in [Table 3](#) (A-K). All cluster mean mass
785 spectra as well as further details on the separation of different clusters are shown in the
786 supplement (Figures [S23-S56](#); Table [S1S2](#)). Further particle types were determined by
787 searching for specific marker peaks, see section 2.4.3.

788 **2.4.2. Uncertainties of clustering by the fuzzy c-means algorithm**

789 By manual inspection of the cluster algorithm results it was found that occasionally mass
790 spectra were classified falsely by the algorithm, depending on cluster number and particle
791 type. To take into account uncertainties of the resulting particle type fractions, the

792 uncertainties were estimated by means of a reduced, representative data set of the HCCT-
793 2010 campaign. For this, 1377 single particle mass spectra were clustered by fuzzy c-means
794 using the same parameters as described above. The resulting clusters were assigned to particle
795 types based on their averaged mass spectrum. Afterwards the individual mass spectra of every
796 particle type were reviewed manually. For example, 274 particle spectra were sorted into the
797 particle type "org, K". The number of mass spectra being assigned falsely to the considered
798 particle type was determined ($\Delta_{\text{false positive}}$). In case of "org, K", 51 mass spectra of this
799 particle type belonged to a different particle type. The number of mass spectra being classified
800 falsely to another particle type was also determined ($\Delta_{\text{false negative}}$). In order to do this, all
801 other clusters were inspected and the number of mass spectra belonging ~~actual~~ to "org, K"
802 was counted. In this example, 43 mass spectra of the particle type "org, K" were assigned to
803 clusters of other particle types by the algorithm. Since both false classifications are not
804 dependent on each other, we chose to apply Gaussian error propagation for the determined
805 uncertainty of a particle type ($\Delta_{\text{particle type}}$):

$$806 \quad \Delta_{\text{particle type}} = \sqrt{\Delta_{\text{false positive}}^2 + \Delta_{\text{false negative}}^2} \quad (3).$$

807 In case of "org, K", $\Delta_{\text{particle type}} = 67$, meaning that the error is about 24% of the absolute
808 number of mass spectra of this cluster. ~~This reduced test set contained~~ ~~Due to the fact that a~~
809 ~~reduced data set was applied, not all particle types were included, because~~ no particles of the
810 type "mineral dust" and "Ca" ~~were present in the test data set~~. The uncertainty for the particle
811 type "Ca" was therefore estimated by averaging the uncertainties of the other particles types,
812 while the particle type "mineral dust" was further refined by the marker method and the
813 uncertainty was inferred as explained in section 2.4.3. Table 2 shows the details of the test
814 data set along with the resulting uncertainties for the different particle types. In this test case,
815 a total of 16% of all mass spectra were assigned to a wrong particle type. In relation to the
816 absolute number of each particle type, $\Delta_{\text{particle type}}$ ranges ~~between~~ 13% and 50%. The largest
817 uncertainties are found for the particle types "diesel exhaust" (50%), "amines" (35%), "soot
818 and org" (31%) and "K" (30%). The large error bar of the fraction "others" can be explained
819 by the exclusion of mass spectra that would have been assigned manually to an existing
820 particle type. The determined uncertainties were adopted for the clustering of the total data
821 set.

822 **2.4.3. Particle type identification by marker peaks**

823 In addition to the clustering method that compares the whole mass spectra of the individual
824 particles, it is also useful to search for certain marker peaks, especially in cases when these
825 peaks are of small intensity such that they do not influence the correlation of two mass spectra
826 and therefor do not show up in the clustering results. A typical example would be looking for
827 metals (e.g., lead) or rarely appearing particle types (Dall'Osto et al., 2004; Tolocka et al.,
828 2004; Snyder et al., 2009). By the marker method it was possible to identify two different
829 particle types characterized by the abundance of iron, namely "mineral dust" and "Fe, V" (iron
830 internally mixed with vanadium). Indicators for mineral dust are besides Fe^+ also Na^+
831 (m/z 23) and K^+ (m/z 39) (Silva et al., 2000; Hinz et al., 2006; Dall'Osto et al., 2010), while
832 Vanadium (V^+ , m/z 51) originates rather from fuel combustion (Tolocka et al., 2004; Korn et
833 al., 2007; Ault et al., 2010) and industrial sources like refineries (Dall'Osto et al., 2004; Ault
834 et al., 2009) than from mineral dust. Details on the classification of iron containing particles
835 | can be found in the supplementary material (Section [34](#), Figure [S76](#)).

836 The method is also suitable for investigating the particle mixing state when looking at the
837 abundance of, e.g., nitrate and sulphate independent of the particle type. Uncertainties for
838 | particle types derived by the marker method were estimated using counting statistics ([square](#)
839 | [root of absolute number of counted particles](#)).

840 **2.4.4. Combined analysis using clustering and marker peaks**

841 In order to optimize the data analysis and as a consequence of the two preceding sections, we
842 chose to apply a combined method of clustering and marker peaks: After the clustering, the
843 fraction "others" has been additionally investigated by marker peaks of lead, nickel,
844 vanadium, and iron. Also the particle type characterized by iron inferred from the clustering
845 method was analysed further using the marker peak method, resulting in two particle types:
846 one interpreted as mineral dust and the other consisting of iron internally mixed with
847 vanadium ("Fe, V"), belonging probably to an industrial source. Using the combined method
848 of clustering and marker peak analysis, a total of 14 particle types plus "others" were
849 identified. A summary of the resulting particle types, the applied method and their
850 characteristic signals for identification as well as the corresponding chemical composition in
851 | the mass spectra are listed in [Table 3](#)~~Table 3~~. Due to the fact that all particle types were
852 internally mixed with secondary inorganic compounds like nitrate and sulphate, these

853 compounds are not explicitly mentioned in the legend. The mean positive and negative mass
854 spectra of the 14 particle types plus the averaged remaining mass spectra ("others") are shown
855 in Figure 2. An overview of all cluster types obtained by the clustering method can be found
856 in the supplement (Figures S23-S56).

857

858 3. Results

859 3.1. Size resolved aerosol composition and identification of local sources

860 Figure 3 shows the size resolved particle composition for all particles (not separated for out-
861 of-cloud aerosol and cloud residues). The relative fraction of all particles in the specific size
862 class is given in order to eliminate the size dependent detection efficiency of the ALABAMA
863 (Brands et al., 2011). The total number of analysed particles per size bin is given by the grey
864 line. The maximum of the analysed particles lies in the size range between 500 and 550 nm,
865 due to the best detection and ablation efficiency of the ALABAMA in this size range. The
866 particle types shown in Figure 3 refer only to the results obtained by the fuzzy c-means
867 clustering, thus the particle types "Fe, V", "Ni", and "Pb" are contained in the type "others".
868 The most abundant particle types are "org, K", "biomass burning" and "soot" (see also Table
869 4). The particle types "diesel exhaust" as well as "soot, org" only appear significantly at small
870 vacuum aerodynamic diameters between 200 and 450 nm. This indicates that these particles
871 were recently emitted and had no time grow by condensation or coagulation. In contrast, the
872 particle types "org", "amines" and "soot", are observed only with diameters larger than 450
873 nm. This agrees with the observation that all analysed soot particles were internally mixed
874 with nitrate and sulphate (see section 3.4) and indicates that these soot particles were aged and
875 have been processed and coated. Particles of the type "biomass burning" and "org, K" are
876 found in all size classes, although the type "org, K" has a clear maximum between 400 and
877 500 nm.

878 Figure 4 shows the number of detected particles as a function of the percentage of particles
879 that were analysed during certain local wind directions at the Schmücke. Panel a) gives the
880 standard wind rose for the whole time period. The dominating wind direction was southwest,
881 with about 50% probability for wind directions between 200 and 270°. This direction
882 corresponds to the requirements for cloud events. The absolute number of detected particles is
883 given in Panel b), showing that the majority of the detected particles were measured when the
884 wind came from southwest. However, as shown in Panel c), per unit of time more particles

885 were detected when the local wind direction was between 0 and 90°. In these directions lie
886 several larger cities (Erfurt, Weimar, Jena, see map in Figure S1) such that in general a higher
887 pollution level may be expected.

888 ~~The graph shows that about 50% of all particles were detected when the wind was coming~~
889 ~~from south-western directions between 180 and 270° and about 25% of the particles were~~
890 ~~detected when the wind came from north-east respectively east (~40°—100°). The wind~~
891 ~~velocities are indicated by the colour code: Wind velocities were higher during south-westerly~~
892 ~~winds (mainly between 10 and 30 km h⁻¹; red and blue), while during north-easterly wind~~
893 ~~directions the wind velocity was mainly between 10 and 20 km h⁻¹ (red). North-westerly and~~
894 ~~south-easterly wind directions were almost not observed at all at the measurement station.~~

895 Several particle types show a distinct diurnal pattern, indicating a source with a specific
896 emission pattern. The fact that the emission pattern is detectable at the measurement site
897 suggests that the source is not too far away, such that the diurnal pattern is not smoothed by
898 different air mass transport velocities and different wind directions. An example is shown in
899 Figure 5. The figure shows the complete time series for the particle type "diesel exhaust"
900 (upper panel) and the averaged diurnal pattern (lower panel). The diurnal pattern shows the
901 increased occurrence of particles of this type between 9:00 and 24:00 and a decrease of this
902 particle type during the night. This indicates the contribution of traffic emissions from within
903 one or two hours from the measurement site (local traffic typically starts around 7:00 in the
904 morning). All clusters contained in each particle type were inspected for such a diurnal trend.
905 From this the amount of particle influences by local or regional sources were obtained. Table
906 4 shows the relative abundance of the particle types during HCCT-2010 along with the
907 percentage of clusters showing diurnal variations and those not showing a diurnal trend. In
908 total, about 63% of the analysed particles belong to clusters indicating a diurnal variation.
909 This finding implies that the aerosol composition during HCCT-2010 is mainly influenced by
910 local and regional sources.

911 **3.2. Comparison of out-of-cloud aerosol and cloud residues**

912 One of the main objectives of this study was the analysis of cloud residues and the
913 comparison to the aerosol composition under cloud-free conditions. Figure 6 shows the
914 average aerosol particle composition for all out-of-cloud aerosol particles and all cloud
915 residues measured during HCCT-2010, not restricted to the full cloud events. It has to be

916 noted that measurements of cloud residues and out-of-cloud aerosol can by definition not be
917 made simultaneously, such that differences in the meteorological condition influences such a
918 comparison. In the following we will compare the relative abundance of the individual
919 particle types between cloud residues and out-of-cloud aerosol:

920 **3.2.1. Organic particle types**

921 For both organic particle types ("org, K" and "org") the relative abundance in cloud residues
922 is smaller than in the out-of-cloud aerosol. This observation may partly be in contradiction
923 with previous measurements reported in the literature. For example, measurements of cloud
924 residue composition by Drewnick et al. (2007) using an Aerodyne AMS reported increased
925 organic mass fractions in cloud residues. However, these measurements are hard to compare
926 because AMS data are based on average aerosol mass while the ALABAMA data are based
927 on single particle ~~type-occurrence~~ analysis. Furthermore, Drewnick et al. (2007) did not
928 consider refractory species in the aerosol composition and did not separate the organic mass
929 into different subgroups. For example, in our study the particle types "soot" and "biomass
930 burning" reveal a significant fraction of the aerosol composition (see below), and aerosol
931 originating from biomass burning can be a significant fraction of the "organic" aerosol mass
932 reported by the AMS (e.g., Lanz et al., 2010; Crippa et al., 2013; Crippa et al., 2014). The
933 AMS data from the HCCT-2010 campaign that are presented in a companion paper
934 (Schneider et al., 2015) show a slightly lower scavenging efficiency for organics than for
935 nitrate and sulphate. In-cloud scavenging of organic particles depends on the solubility of the
936 organic compounds (Limbeck and Puxbaum, 2000). The slightly lower scavenging efficiency
937 may therefore be explained by the lower solubility of hydrophobic organic compounds like
938 aromatics whose fragments were frequently observed our single particle mass spectra ($C_4H_3^+$
939 (m/z 51), $C_6H_5^+$ (m/z 77), $C_9H_7^+$ (m/z 115), see mass spectrum "org, K_2" in Figure S32).

940 **3.2.2. Amine-containing particles**

941 Several characteristic peaks for amines have been reported in the literature, the most common
942 appear to be m/z 59 ($(CH_3)_3N^+$) and m/z 74 ($(C_2H_5)_2NH_2^+$) (Angelino et al., 2001; Pratt et al.,
943 2009; Rehbein et al., 2011; Zhang et al., 2012; Healy et al., 2014a). We observed a particle
944 type with the abundance of m/z 59 and to a lesser degree also m/z 74 (Figure 2) that we
945 interpret as organic particle containing amines. In addition, the fragmentation patterns of
946 several single particle mass spectra show ~~further~~ peaks at m/z 86 ($(C_2H_5)_2NCH_2^+$) and m/z

947 | 101 (molecular peak of trimethylamine, TMA) indicating detection of TMA (Angelino et al.,
948 | 2001). Interestingly, the relative fraction of mass spectra containing signatures for amines is
949 | increased in the cloud residues (Figure 6). Thus, the time series of the characteristic marker
950 | peak m/z 59 was compared to the concentrations of ~~trimethylamine~~ (TMA), dimethylamine
951 | (DMA) and methylamine (MA) measured in the cloud water samples by ion chromatography
952 | (Figure 7). Caution is required because cobalt is an isobar to the amine fragment $(\text{CH}_3)_3\text{N}^+$ at
953 | m/z 59. But since cobalt was detected during HCCT-2010 only in very low concentration in
954 | the cloud water samples (Fomba et al., 2015), we ascribe the signal at m/z 59 to amine
955 | compounds. Due to the fact that cloud water sampling was not done continuously, the time
956 | series of ALABAMA and the amine species are only partly comparable. A reasonably good
957 | agreement is observed between the number of amine containing mass spectra per hour and the
958 | mass concentration of TMA (Pearson's $r = 0.60$) except for the disagreement around 17:00.
959 | Amine compounds in the atmosphere can originate from various sources (Ge et al., 2011).
960 | Besides from animal husbandry and biomass burning (Schade and Crutzen, 1995), TMA,
961 | DMA and MA can originate from, e.g., industrial processes (Ge et al., 2011) and have been
962 | observed in ambient air (Chang et al., 2003; Sellegri et al., 2005). An enhanced partitioning
963 | for gas phase trimethylamine (TMA) on pre-existing particles coated by an aqueous layer was
964 | observed at high relative humidity and low temperature (Rehbein et al., 2011; Zhang et al.,
965 | 2012), thus the generally increased abundance of amines in cloud water may not be
966 | surprising. Whether amines remain in the aerosol phase after cloud droplet evaporation
967 | remains unclear, but may play an important role in cloud processing of aerosol particles.

968 **3.2.3. Biomass burning and soot**

969 | The results also show an increased fraction of the particle type "soot" in cloud residues.
970 | Freshly emitted soot particles are hydrophobic and do not serve as CCN at realistic
971 | supersaturations (Dusek et al., 2006a; Koehler et al., 2009). Nevertheless, it was observed in
972 | several studies that soot is more efficiently activated than organic particles (Hitzenberger et
973 | al., 2000; Sellegri et al., 2003). The size resolved aerosol composition (see Figure 3) shows
974 | that the observed "soot" particles were mainly larger than 450 nm, leading to the conclusion
975 | that mostly aged soot particles were analysed by the mass spectrometer. Furthermore, the
976 | "soot" clusters reveal internal mixtures with soluble inorganic compounds like nitrate or
977 | sulphate, which is presumably leading to activation of these particles at lower critical
978 | supersaturation (Dusek et al., 2006a; Henning et al., 2010). Internally mixed particles can

979 either develop from condensation of secondary compounds on pre-existing particles or from
980 coagulation with hygroscopic particles respectively cloud droplets. Due to the fact that even
981 the out-of-cloud aerosol particles that contain soot are internally mixed with secondary
982 inorganic compounds, the increased fraction of soot particles in cloud residues can rather be
983 explained by a good CCN activity of hygroscopic soot particles than caused by in-cloud
984 impaction scavenging. Aging of atmospheric soot particles by coating with sulphate and
985 nitrate has been observed using single particle mass spectrometry by Pratt and Prather (2010)
986 as well as by Moffet and Prather (2009). The authors concluded that such processing of soot
987 particles in the urban environment of Mexico City takes about three hours. Although in a
988 cleaner environment than Mexico City coating by nitrate and sulphate will likely be slower, it
989 appears to be a reasonable explanation for the findings that soot-containing particles internally
990 mixed with nitrate and sulphate are efficiently activated as CCN and are therefore enhanced in
991 cloud residues. [Similar findings have been reported for growth factors of coated black carbon
992 particles measured in Paris using a hygroscopic tandem differential mobility analyser and a
993 single particle mass spectrometer](#) (Healy et al., 2014b). The mass based scavenging efficiency
994 [of soot particles in our study](#) was found to be markedly lower than that of sulphate or nitrate
995 (Schneider et al., 2015), confirming the assumption that the large soot-containing particles (>
996 450 nm) found in the cloud residues contain soot only as a minor mass fraction.

997 The relative percentage of biomass burning particles occurring in the out-of-cloud aerosol
998 does not differ much from that in the cloud residues. In agreement with previous observations
999 (Ross et al., 2003; de Villiers et al., 2010) this implies that aerosol from biomass burning is an
1000 effective CCN, resulting from a high content of soluble organic and inorganic compounds in
1001 the particles (Silva et al., 1999; Posfai et al., 2003; Andreae and Rosenfeld, 2008; Pratt et al.,
1002 2011).

1003 The high percentage of particles originating from combustion processes ("soot", "biomass
1004 burning", "diesel exhaust") of about 43 % (Figure 6) is investigated more closely in the
1005 following. Figure 8 shows the time series of the particle types "soot" (blue, Figure 8b) and the
1006 sum of all particle types containing elemental carbon (brown, Figure 8c) observed by
1007 ALABAMA, along with temperature, concentration of equivalent black carbon (EBC)
1008 measured by the MAAP, and the biomass burning aerosol inferred from AMS data (green,
1009 Figure 8d). The latter was estimated from the AMS data based on the marker peak at m/z 60
1010 for Levoglucosan which is an indicator for biomass burning (Simoneit et al., 1999; Schneider

1011 et al., 2006; Alfarra et al., 2007). Conversion of f_{60} (fraction of m/z 60 in the total organic
1012 signal) into mass concentration was demonstrated by Weimer (2008) and Crippa et al. (2014).
1013 The time series of the "soot" particle type agrees only partly with the time series of EBC. A
1014 better agreement ($r = 0.47$) is reached if the time series of all clusters containing elemental
1015 carbon in the mean mass spectra ("soot", "diesel exhaust", "biomass burning") is compared to
1016 EBC. The three data sets (MAAP, ALABAMA, AMS) allow for the attribution of the events
1017 shown in Figure 8 with enhanced EBC concentrations to different particle types: The event on
1018 24 September 2010 (blue frame) is not caused by biomass burning but from combustion of
1019 other (most likely fossil) fuel (like coal, oil, diesel), because the biomass burning marker
1020 remains low. In contrast, the events from 10 October 2010 to 15 October 2010 and from 17
1021 October 2010 to 19 October 2010 (green frame) can be mainly attributed to biomass burning.
1022 The short data gap on 17 October is due to technical issues. Furthermore the EBC
1023 concentration and the percentage of biomass burning particles rise with decreasing
1024 temperature (Figure 8a). This can be attributed to the beginning of heating period and
1025 consequently increased heating after 1 October 2010 leading to increased emission of from
1026 local and regional residential heating in the city Suhl and other smaller cities and villages in
1027 south-westerly direction (compare also Section 3.3).

1028

1029 **3.2.4. Mineral dust and metals**

1030 Except for the particle type "Ca", the number fractions of mineral dust and metallic particle
1031 types ("Fe, V", "Ni" and "Pb") are markedly enhanced in the cloud residues. All these
1032 particles contain nitrate and sulphate, too (see Figure 2), thus the good activation or
1033 scavenging efficiency is likely caused by the soluble compounds in these particles. The
1034 presence of metals in cloud droplets has important implications for the oxidation of sulphur
1035 containing species in the aqueous phase. Catalytic oxidation of SO₂ to sulphate by transition
1036 metals as Fe and Mn (Calvert et al., 1985), but also Ti (Harris et al., 2013) and V (Ault et al.,
1037 2010) is a process that has long been recognized (Calvert et al., 1985; Bradbury et al., 1999),
1038 but data obtained during HCCT2010 have shown that this process is of higher importance
1039 than previously thought (Harris et al., 2013). In marine environments, dimethyl sulphide can
1040 be catalytically oxidized by vanadium to methanesulphonic acid (Gaston et al., 2010).
1041 Enrichment of these transition metals in cloud droplets may be explained by cloud processing:
1042 Transition metal-catalysed sulphate production in the cloud droplets leads to a higher sulphate

1043 content of the metal-containing aerosol particles remaining after cloud evaporation and
1044 thereby to a better activation of these particles in the next cloud formation process.
1045

1046 **3.3. Cloud residue analysis for the full cloud events (FCE)**

1047 In the following the selected full cloud events (see Table 1) will be analysed in more detail.
1048 These cloud events represent a subset of all cloud measurements and are referring to certain
1049 conditions that were given in detail in Tilgner et al. (2014). The composition of the cloud
1050 residual particles measured during the individual FCE during HCCT-2010 are shown in
1051 Figure 9. Also given are the number of analysed mass spectra and the averaged mass
1052 concentration of equivalent black carbon measured in the interstitial aerosol during the events.
1053 Only FCE with sufficient (> 100) number of mass spectra are considered. These individual
1054 events show large event-to-event variability, especially in the fraction of particles of the type
1055 "soot". Four FCE are characterized by a markedly higher fraction of "soot" particles, namely
1056 FCE 7.1, 11.2, 11.3 and 13.3, all of them between 24 September and 06 October. These
1057 events are also characterised by a high absolute mass concentration of EBC, especially FCE
1058 11.2 and FCE 13.3 with about 300 ng m^{-3} of EBC. To further investigate this finding, the
1059 origin of the air masses encountered during these FCE is inspected by means of back
1060 trajectories. Figure 10 displays the 96h-back trajectories, separated for the "low-soot FCE"
1061 (left) and the "high-soot FCE" (right). It becomes clear that the air masses encountered during
1062 the "low-soot FCE" arrive mainly from west/north west and have spent a considerable amount
1063 of the 96 hours prior to the measurement over the Atlantic Ocean (see also Figure S1 in the
1064 supplementary material to Tilgner et al. (2014)). These air masses had less opportunity to
1065 accumulate pollution particles over the continent. In contrast, the "high-soot" air masses
1066 arrive more from south/south-west and have travelled slower, therefore having spent more
1067 time of the previous 96 hours of land, leading to higher accumulation of anthropogenic
1068 emitted particles like soot. An exceptional case is FCE 22.0 (included in the left graph of
1069 Figure 10), where the air masses arrive from east/north-east, although the local wind direction
1070 was south-west (as a prerequisite for an FCE). This air mass contained the highest fraction of
1071 biomass burning particles of all FCE and the highest number of mass spectra per event and
1072 time (1561 spectra in only 7.2 hours, see Table 1). It has to be noted here that the full cloud
1073 events may not be representative for the general situation for clouds at the Schmücke, because
1074 of the selected data set. The composition data for the FCE are based on 4400 mass spectra,

1075 while for the composition of all cloud residues (Figure 6) more than 13000 mass spectra were
1076 analysed. For example, the required prerequisite that the local wind direction for an FCE has
1077 to be south-west, air masses of all FCE pass the city of Suhl located south-west of the
1078 Schmücke, which may lead to a higher relative amount of anthropogenic particles and a
1079 higher influence of local and regional emissions in the full cloud events compared to the
1080 general case. On the other hand, the analysis of the diurnal cycles in section 3.1 has shown
1081 that in general local and regional sources have a high influence on the aerosol particle
1082 abundance.

1083 **3.4. Change of particle mixing state by cloud processing**

1084 As mentioned before, all identified particle types indicate internal mixtures with nitrate,
1085 sulphate or both species. Therefore the clustering algorithm can't provide information about
1086 the particle mixing state from out-of-cloud to inside of the cloud. Therefore, the mixing state
1087 of the particles with nitrate and sulphate was investigated by means of the characteristic
1088 marker peaks m/z -62 (NO_3^-) and m/z -97 (HSO_4^-).

1089 To compare cloud residues and out-of-cloud aerosol, we selected air masses with comparable
1090 origins based on HYSPLIT back trajectories for in-cloud and out-of-cloud conditions. As an
1091 additional criterion it was required that the local wind direction at the Schmücke was
1092 constant. The listed events "I" and "II" in Table 5 fulfilled these criteria. These events differ
1093 slightly from the defined FCEs because the criteria for the FCEs were not taken into account
1094 here. The cloud sampling phase of event "I" corresponds mostly to FCE1.1, while that of
1095 event "II" is a part of FCE24.0. During event "I" the air masses for in-cloud and out-of-cloud
1096 conditions both arrived from France, while air masses for both conditions during event "II"
1097 passed over England.

1098 The characteristic marker peaks m/z -62 and m/z -97 in the single particle mass spectra of the
1099 events "I" and "II" show that only less than 1% of the out-of-cloud aerosol particles contained
1100 neither nitrate nor sulphate for both events. Thus, 99% of the out-of-cloud aerosol particles
1101 were already internally mixed with secondary inorganic compounds before passing the cloud.
1102 Such a high percentage of particles being internally mixed with secondary inorganic
1103 compounds were also found by single particle mass spectrometry during other studies in
1104 California (Cahill et al., 2012) or Harrow (Jeong et al., 2011). However, we observed an
1105 increase of the particle fraction containing nitrate in the cloud residues compared to the out-

1106 of-cloud aerosol, and the same finding holds for sulphate (Figure 11, left). This can be
1107 explained by a more detailed analysis of the particle mixing state, distinguishing between
1108 particles containing only nitrate, only sulphate or both nitrate and sulphate (Figure 11, right).
1109 Particles internally mixed only with sulphate (i.e. containing no nitrate) represent in general a
1110 minor fraction (< 3%). For both analysed events the percentage of particles containing only
1111 nitrate and only sulphate was smaller in case of cloud residues compared to the out-of-cloud
1112 aerosol while the percentage of particles with nitrate and sulphate was increased. This
1113 observed increase indicates a sulphate addition to those particles that contained only nitrate,
1114 but also a nitrate addition to those particles that contained only sulphate. In the cloud residues,
1115 particles not containing nitrate can almost not be found. It must be noted that relative
1116 percentages of out-of-cloud aerosol particles internally mixed with secondary inorganics
1117 added for both events are less than the 99% inferred above, due to the different threshold
1118 values that had to be used for the definition whether a peak is present in a mass spectrum or
1119 not (see supplement, chapter 3). This addition of sulphate and nitrate (and possibly also of
1120 organic components as amines, see 3.2.2) by cloud processing can also be observed in a size
1121 shift of the analysed particles. Figure 12 shows the size histograms of the particles analysed
1122 by ALABAMA during event I and II. In both cases a shift in the histogram to larger sizes is
1123 observed. The activation of CCN to cloud droplets is usually occurring at much smaller sizes
1124 (activation diameters upwind of the Schmücke have been observed to range between 123 and
1125 194 nm (Henning et al., 2014)), such that the observed size shift by ALABAMA can very
1126 likely be attributed to the uptake of gaseous species by the cloud droplets, leading to a size
1127 increase of the residual particles.

1128 These two case studies demonstrate the change of the particle mixing state by chemical
1129 processes inside the cloud liquid phase. Similar observations were found earlier in numerous
1130 studies (e.g., Laj et al., 1997b; Sellegri et al., 2003; Brüggemann et al., 2005; McFiggans et
1131 al., 2006; Hayden et al., 2008; Zelenyuk et al., 2010). The enrichment of nitrate was also
1132 observed by simultaneous measurements with an AMS providing evidence of an increased
1133 mass concentration of nitrate in cloud residues compared to interstitial and out-of-cloud
1134 aerosol (Schneider et al., 2015). Such an enhancement of nitrate in cloud droplets can be
1135 explained by the uptake of gaseous nitric acid into the cloud droplets (Tilgner et al., 2005;
1136 Hayden et al., 2008). Enrichment of sulphate in cloud droplets can occur via different
1137 pathways. Besides the uptake of gaseous H₂SO₄ and the scavenging of ultrafine particulate
1138 matter also the uptake of SO₂ with subsequent oxidation plays a role (Harris et al., 2014).

1139 Furthermore Harris et al. (2013) could prove that besides the known SO₂ oxidation by H₂O₂
1140 also the oxidation with O₂ catalysed by transition metals plays a significant role for the
1141 sulphate production. Despite the low number concentration of activated mineral dust particles
1142 in general, it became apparent that SO₂ oxidation was mainly catalysed by dissolved transition
1143 metals during HCCT-2010. As it was shown in this study, transition metals were also detected
1144 by the ALABAMA (see Table 2).

1145 Furthermore the aerosol hygroscopicity was investigated in the same field experiment before
1146 and after cloud formation at the valley sites. In agreement with the described results, the
1147 hygroscopicity of the particles was found to be increased after passing the cloud (up to 50%,
1148 see Henning et al. (2014). By means of the above described processes water-soluble material
1149 is enriched inside the particles while being processed by the cloud. After evaporation of the
1150 cloud the water-soluble material it is likely to remain in the particles, thereby increasing their
1151 hygroscopicity. This process will occur in all cloud droplets formed from all CCN sizes, and
1152 therefore also influence the CCN properties of aerosol particles smaller than analysed here.
1153 For small aerosol particles that are in the size range of the activation diameter for a specific
1154 supersaturation the chemical composition plays an important role for the activation.

1155 **4. Summary and Conclusions**

1156 During the HCCT-2010 campaign, more than 170 000 aerosol particles and more than 14 000
1157 cloud residual particles were analysed by single particle mass spectrometry. The data
1158 evaluation was done by a combination of the clustering algorithm fuzzy c-means and the
1159 marker peak method, resulting in 14 different particle types. From the diurnal trends of the
1160 occurrence of these particle types, the influence of local and regional sources on the aerosol
1161 composition was estimated to be about 63%. Especially the particle types "soot" and "biomass
1162 burning" could be allocated to local or regional sources. The single particle data further
1163 allowed for a better attribution of equivalent black carbon to different sources, as fossil fuel
1164 burning or biomass burning. Important local sources are the city Suhl in the predominant
1165 wind direction, together with the beginning of the heating period in October, leading to
1166 increased biomass burning signatures.

1167 Analysis of the cloud residues revealed that the relative percentage of soot and amines is
1168 increased compared to out-of-cloud aerosol. Analysis of cloud water samples by ion
1169 chromatography showed that amines were mainly found in the form of trimethylamine. The
1170 increased fraction of soot can be explained by processing of soot particles leading to coating

1171 by nitrate and sulphate which is known to occur in a few hours. In addition the size resolved
1172 aerosol composition reveals that the detected particles containing soot are larger than 450 nm.
1173 Both facts suggest that such processed soot particles are good cloud condensation nuclei.

1174 All observed particle types show internal mixtures with the secondary inorganic compounds
1175 nitrate and/or sulphate. By means of the characteristic marker peaks m/z -62 and m/z -97 for
1176 nitrate respectively sulphate, the change of the particle mixing state from out-of-cloud to in-
1177 cloud was investigated in two case studies. In both cases the addition of nitrate and sulphate
1178 to the cloud droplets was observed. This finding is most likely due to the uptake of HNO_3
1179 from the gas phase and sulphate production by the oxidation of SO_2 by transition metals and
1180 H_2O_2 inside the cloud droplets (Harris et al., 2014), besides the uptake of H_2SO_4 .

1181 Such a cloud processing of aerosol particles has important implications for the hygroscopic
1182 properties of the aerosol particles after cloud passage. An increase of soluble compounds in
1183 the particles, together with the involved growth of the particle size, will lead to an enhanced
1184 number of CCN that are available in the air mass after evaporation of the cloud. Additionally
1185 the modified chemical composition can lead to altered radiation properties concerning light
1186 scattering and absorption. Especially internal mixed soot particles indicate a higher absorption
1187 than pure soot particles (Jacobson, 2001) and could therefore counteract the cooling effect of
1188 clouds.

1189

1190 **Acknowledgments**

1191 The German Research Foundation DFG funded the participation of S. Mertes (grant HE
1192 939/25-1 and ME 3534/1-2).

1193 We thank Thomas Böttger, Wilhelm Schneider, Paul Reitz, Jovana Diesch, Sarah-Lena von
1194 der Weiden-Reinmüller and Friederike Freutel for the support at the measurement site as well
1195 as Frank Helleis for electrical and technical advices and the whole HCCT-2010 team.

1196

1197

1198 **References**

1199

1200 Alfarra, M. R., Prevot, A. S. H., Szidat, S., Sandradewi, J., Weimer, S., Lanz, V. A.,
1201 Schreiber, D., Mohr, M., and Baltensperger, U.: Identification of the mass spectral

signature of organic aerosols from wood burning emissions, *Environ. Sci. Technol.*,
 41, 5770-5777, 10.1021/es062289b, 2007.

Allan, J. D., Baumgardner, D., Raga, G. B., Mayol-Bracero, O. L., Morales-Garcia, F.,
 Garcia-Garcia, F., Montero-Martinez, G., Borrmann, S., Schneider, J., Mertes, S.,
 Walter, S., Gysel, M., Dusek, U., Frank, G. P., and Kramer, M.: Clouds and aerosols
 in Puerto Rico - a new evaluation, *Atmospheric Chemistry and Physics*, 8, 1293-1309,
 2008.

Andreae, M. O., and Rosenfeld, D.: Aerosol-cloud-precipitation interactions. Part 1. The
 nature and sources of cloud-active aerosols, *Earth-Science Reviews*, 89, 13-41,
 10.1016/j.earscirev.2008.03.001, 2008.

Angelino, S., Suess, D. T., and Prather, K. A.: Formation of aerosol particles from reactions
 of secondary and tertiary alkylamines: Characterization by aerosol time-of-flight mass
 spectrometry, *Environ. Sci. Technol.*, 35, 3130-3138, 10.1021/es0015444, 2001.

Ault, A. P., Moore, M. J., Furutani, H., and Prather, K. A.: Impact of Emissions from the Los
 Angeles Port Region on San Diego Air Quality during Regional Transport Events,
Environ. Sci. Technol., 43, 3500-3506, 10.1021/es8018918, 2009.

Ault, A. P., Gaston, C. J., Wang, Y., Dominguez, G., Thiemens, M. H., and Prather, K. A.:
 Characterization of the Single Particle Mixing State of Individual Ship Plume Events
 Measured at the Port of Los Angeles, *Environ. Sci. Technol.*, 44, 1954-1961,
 10.1021/es902985h, 2010.

Bein, K. J., Zhao, Y. J., Wexler, A. S., and Johnston, M. V.: Speciation of size-resolved
 individual ultrafine particles in Pittsburgh, Pennsylvania, *J. Geophys. Res.-Atmos.*,
 110, 10.1029/2004jd004708, 2005.

Bezdek, J. C.: *Pattern Recognition with Fuzzy Objective Function Algorithms*, Plenum Press,
 New York, 1981.

Bezdek, J. C., Ehrlich, R., and Full, W.: FCM - The fuzzy c-means clustering-algorithm,
Comput. Geosci., 10, 191-203, 10.1016/0098-3004(84)90020-7, 1984.

Bower, K. N., Hill, T. A., Coe, H., and Choulaton, T. W.: SO₂ oxidation in an entraining
 cloud model with explicit microphysics, *Atmospheric Environment Part a-General
 Topics*, 25, 2401-2418, 10.1016/0960-1686(91)90114-m, 1991.

Bower, K. N., Choulaton, T. W., Gallagher, M. W., Colvile, R. N., Wells, M., Beswick, K.
 M., Wiedensohler, A., Hansson, H. C., Svenningsson, B., Swietlicki, E., Wendisch,
 M., Berner, A., Kruisz, C., Laj, P., Facchini, M. C., Fuzzi, S., Bizjak, M., Dollard, G.,
 Jones, B., Acker, K., Wieprecht, W., Preiss, M., Sutton, M. A., Hargreaves, K. J.,
 Storeton-West, R. L., Cape, J. N., and Arends, B. G.: Observations and modelling of
 the processing of aerosol by a hill cap cloud, *Atmos. Environ.*, 31, 2527-2543,
[http://dx.doi.org/10.1016/S1352-2310\(96\)00317-2](http://dx.doi.org/10.1016/S1352-2310(96)00317-2), 1997.

Bradbury, C., Bower, K. N., Choulaton, T. W., Swietlicki, E., Birmili, W., Wiedensohler, A.,
 Yuskiewicz, B., Berner, A., Dusek, U., Dore, C., and McFadyen, G. G.: Modelling of
 aerosol modification resulting from passage through a hill cap cloud, *Atmos. Res.*, 50,
 185-204, [http://dx.doi.org/10.1016/S0169-8095\(98\)00104-5](http://dx.doi.org/10.1016/S0169-8095(98)00104-5), 1999.

Brands, M., Kamphus, M., Böttger, T., Schneider, J., Drewnick, F., Roth, A., Curtius, J.,
 Voigt, C., Borbon, A., Beekmann, M., Bourdon, A., Perrin, T., and Borrmann, S.:
 Characterization of a Newly Developed Aircraft-Based Laser Ablation Aerosol Mass
 Spectrometer (ALABAMA) and First Field Deployment in Urban Pollution Plumes
 over Paris During MEGAPOLI 2009, *Aerosol Sci. Technol.*, 45, 46-64,
 10.1080/02786826.2010.517813, 2011.

Brüggemann, E., Gnauk, T., Mertes, S., Acker, K., Auel, R., Wieprecht, W., Moller, D.,
 Collett, J. L., Chang, H., Galgon, D., Chemnitzer, R., Rud, C., Junek, R.,

1251 Wiedensohler, W., and Herrmann, H.: Schmucke hill cap cloud and valley stations
1252 aerosol characterisation during FEBUKO (I): Particle size distribution, mass, and main
1253 components, *Atmos. Environ.*, 39, 4291-4303, 10.1016/j.atmosenv.2005.02.013, 2005.

1254 Cahill, J. F., Suski, K., Seinfeld, J. H., Zaveri, R. A., and Prather, K. A.: The mixing state of
1255 carbonaceous aerosol particles in northern and southern California measured during
1256 CARES and CalNex 2010, *Atmospheric Chemistry and Physics*, 12, 10989-11002,
1257 10.5194/acp-12-10989-2012, 2012.

1258 Calvert, J. G., Lazrus, A., Kok, G. L., Heikes, B. G., Walega, J. G., Lind, J., and Cantrell, C.
1259 A.: Chemical mechanisms of acid generation in the troposphere, *Nature*, 317, 27-35,
1260 10.1038/317027a0, 1985.

1261 Chang, I. H., Lee, C. G., and Lee, D. S.: Development of an automated method for
1262 simultaneous determination of low molecular weight aliphatic amines and ammonia in
1263 ambient air by diffusion scrubber coupled to ion chromatography, *Anal. Chem.*, 75,
1264 6141-6146, 10.1021/ac0347314, 2003.

1265 Corbin, J. C., Rehbein, P. J. G., Evans, G. J., and Abbatt, J. P. D.: Combustion particles as ice
1266 nuclei in an urban environment: Evidence from single-particle mass spectrometry,
1267 *Atmos. Environ.*, 51, 286-292, 10.1016/j.atmosenv.2012.01.007, 2012.

1268 Crippa, M., DeCarlo, P. F., Slowik, J. G., Mohr, C., Heringa, M. F., Chirico, R., Poulain, L.,
1269 Freutel, F., Sciare, J., Cozic, J., Di Marco, C. F., Elsasser, M., Nicolas, J. B.,
1270 Marchand, N., Abidi, E., Wiedensohler, A., Drewnick, F., Schneider, J., Borrmann, S.,
1271 Nemitz, E., Zimmermann, R., Jaffrezo, J. L., Prevot, A. S. H., and Baltensperger, U.:
1272 Wintertime aerosol chemical composition and source apportionment of the organic
1273 fraction in the metropolitan area of Paris, *Atmospheric Chemistry and Physics*, 13,
1274 961-981, 10.5194/acp-13-961-2013, 2013.

1275 Crippa, M., Canonaco, F., Lanz, V. A., Aijala, M., Allan, J. D., Carbone, S., Capes, G.,
1276 Ceburnis, D., Dall'Osto, M., Day, D. A., DeCarlo, P. F., Ehn, M., Eriksson, A.,
1277 Freney, E., Ruiz, L. H., Hillamo, R., Jimenez, J. L., Junninen, H., Kiendler-Scharr, A.,
1278 Kortelainen, A. M., Kulmala, M., Laaksonen, A., Mensah, A., Mohr, C., Nemitz, E.,
1279 O'Dowd, C., Ovadnevaite, J., Pandis, S. N., Petaja, T., Poulain, L., Saarikoski, S.,
1280 Sellegri, K., Swietlicki, E., Tiitta, P., Worsnop, D. R., Baltensperger, U., and Prevot,
1281 A. S. H.: Organic aerosol components derived from 25 AMS data sets across Europe
1282 using a consistent ME-2 based source apportionment approach, *Atmospheric
1283 Chemistry and Physics*, 14, 6159-6176, 10.5194/acp-14-6159-2014, 2014.

1284 Dall'Osto, M., Beddows, D. C. S., Kinnersley, R. P., Harrison, R. M., Donovan, R. J., and
1285 Heal, M. R.: Characterization of individual airborne particles by using aerosol time-of-
1286 flight mass spectrometry at Mace Head, Ireland, *J. Geophys. Res.-Atmos.*, 109,
1287 10.1029/2004jd004747, 2004.

1288 Dall'Osto, M., and Harrison, R. M.: Chemical characterisation of single airborne particles in
1289 Athens (Greece) by ATOFMS, *Atmos. Environ.*, 40, 7614-7631,
1290 10.1016/j.atmosenv.2006.06.053, 2006.

1291 Dall'Osto, M., Harrison, R. M., Coe, H., Williams, P. I., and Allan, J. D.: Real time chemical
1292 characterization of local and regional nitrate aerosols, *Atmospheric Chemistry and
1293 Physics*, 9, 3709-3720, 2009.

1294 Dall'Osto, M., Harrison, R. M., Highwood, E. J., O'Dowd, C., Ceburnis, D., Querol, X., and
1295 Achterberg, E. P.: Variation of the mixing state of Saharan dust particles with
1296 atmospheric transport, *Atmos. Environ.*, 44, 3135-3146,
1297 10.1016/j.atmosenv.2010.05.030, 2010.

1298 de Villiers, R. A., Ancellet, G., Pelon, J., Quennehen, B., Schwarzenboeck, A., Gayet, J. F.,
1299 and Law, K. S.: Airborne measurements of aerosol optical properties related to early

1300 spring transport of mid-latitude sources into the Arctic, *Atmos. Chem. Phys.*, 10,
1301 5011-5030, 10.5194/acp-10-5011-2010, 2010.

1302 DeCarlo, P. F., Kimmel, J. R., Trimborn, A., Northway, M. J., Jayne, J. T., Aiken, A. C.,
1303 Gonin, M., Fuhrer, K., Horvath, T., Docherty, K. S., Worsnop, D. R., and Jimenez, J.
1304 L.: Field-deployable, high-resolution, time-of-flight aerosol mass spectrometer, *Anal.*
1305 *Chem.*, 78, 8281-8289, 10.1021/ac061249n, 2006.

1306 Draxler, R. R., and Rolph, G. D.: HYSPLIT (HYbrid Single-Particle Lagrangian Integrated
1307 Trajectory) Model access via NOAA ARL READY Website
1308 (<http://ready.arl.noaa.gov/HYSPLIT.php>), NOAA Air Resources Laboratory, Silver
1309 Spring, MD, 2012.

1310 Drewnick, F., Hings, S. S., DeCarlo, P., Jayne, J. T., Gonin, M., Fuhrer, K., Weimer, S.,
1311 Jimenez, J. L., Demerjian, K. L., Borrmann, S., and Worsnop, D. R.: A new time-of-
1312 flight aerosol mass spectrometer (TOF-AMS) - Instrument description and first field
1313 deployment, *Aerosol Science and Technology*, 39, 637-658,
1314 10.1080/02786820500182040, 2005.

1315 Drewnick, F., Schneider, J., Hings, S. S., Hock, N., Noone, K., Targino, A., Weimer, S., and
1316 Borrmann, S.: Measurement of ambient, interstitial, and residual aerosol particles on a
1317 mountaintop site in central Sweden using an aerosol mass spectrometer and a CVI, *J.*
1318 *Atmos. Chem.*, 56, 1-20, 2007.

1319 Dusek, U., Reischl, G. P., and Hitztenberger, R.: CCN Activation of Pure and Coated Carbon
1320 Black Particles, *Environ. Sci. Technol.*, 40, 1223-1230, 10.1021/es0503478, 2006a.

1321 Dusek, U., Frank, G. P., Hildebrandt, L., Curtius, J., Schneider, J., Walter, S., Chand, D.,
1322 Drewnick, F., Hings, S., Jung, D., Borrmann, S., and Andreae, M. O.: Size matters
1323 more than chemistry for cloud-nucleating ability of aerosol particles, *Science*, 312,
1324 1375-1378, 2006b.

1325 Facchini, M. C., Decesari, S., Rinaldi, M., Carbone, C., Finessi, E., Mircea, M., Fuzzi, S.,
1326 Moretti, F., Tagliavini, E., Ceburnis, D., and O'Dowd, C. D.: Important Source of
1327 Marine Secondary Organic Aerosol from Biogenic Amines, *Environ. Sci. Technol.*,
1328 42, 9116-9121, 10.1021/es8018385, 2008.

1329 Fomba, K. W., van Pinxteren, D., Müller, K., Iinuma, Y., Lee, T., Collet Jr, J., and Herrmann,
1330 H.: Trace metal characterization of aerosol particles and cloud water during HCCT
1331 2010, *Atmos. Chem. Phys. Discuss.*, 15, 10899-10938, 10.5194/acpd-15-10899-2015,
1332 2015.

1333 Fuzzi, S., Facchini, M. C., Schell, D., Wobrock, W., Winkler, P., Arends, B. G., Kessel, M.,
1334 Möls, J. J., Pahl, S., Schneider, T., Berner, A., Solly, I., Kruisz, C., Kalina, M.,
1335 Fierlinger, H., Hallberg, A., Vitali, P., Santoli, L., and Tigli, G.: Multiphase chemistry
1336 and acidity of clouds at Kleiner Feldberg, *J. Atmos. Chem.*, 19, 87-106,
1337 10.1007/BF00696584, 1994.

1338 Gaston, C. J., Pratt, K. A., Qin, X., and Prather, K. A.: Real-Time Detection and Mixing State
1339 of Methanesulfonate in Single Particles at an Inland Urban Location during a
1340 Phytoplankton Bloom, *Environ. Sci. Technol.*, 44, 1566-1572, 10.1021/es902069d,
1341 2010.

1342 Ge, X., Wexler, A. S., and Clegg, S. L.: Atmospheric amines - Part I. A review, *Atmos.*
1343 *Environ.*, 45, 524-546, 10.1016/j.atmosenv.2010.10.012, 2011.

1344 Gieray, R., Wieser, P., Engelhardt, T., Swietlicki, E., Hansson, H. C., Mentes, B., Orsini, D.,
1345 Martinsson, B., Svenningsson, B., Noone, K. J., and Heintzenberg, J.: Phase
1346 partitioning of aerosol constituents in cloud based on single-particle and bulk analysis,
1347 *Atmos. Environ.*, 31, 2491-2502, [http://dx.doi.org/10.1016/S1352-2310\(96\)00298-1](http://dx.doi.org/10.1016/S1352-2310(96)00298-1),
1348 1997.

1349 Gunthe, S. S., King, S. M., Rose, D., Chen, Q., Roldin, P., Farmer, D. K., Jimenez, J. L.,
 1350 Artaxo, P., Andreae, M. O., Martin, S. T., and Poschl, U.: Cloud condensation nuclei
 1351 in pristine tropical rainforest air of Amazonia: size-resolved measurements and
 1352 modeling of atmospheric aerosol composition and CCN activity, *Atmospheric
 1353 Chemistry and Physics*, 9, 7551-7575, 2009.

1354 Hallberg, A., Ogren, J. A., Noone, K. J., Okada, K., Heintzenberg, J., and Svenningsson, I. B.:
 1355 The influence of aerosol particle composition on cloud droplet formation, *J. Atmos.
 1356 Chem.*, 19, 153-171, 10.1007/BF00696587, 1994.

1357 Harris, E., Sinha, B., van Pinxteren, D., Tilgner, A., Fomba, K. W., Schneider, J., Roth, A.,
 1358 Gnauk, T., Fahlbusch, B., Mertes, S., Lee, T., Collett, J., Foley, S., Borrmann, S.,
 1359 Hoppe, P., and Herrmann, H.: Enhanced Role of Transition Metal Ion Catalysis
 1360 During In-Cloud Oxidation of SO₂, *Science*, 340, 727-730, 10.1126/science.1230911,
 1361 2013.

1362 Harris, E., Sinha, B., van Pinxteren, D., Schneider, J., Poulain, L., Collett, J., D'Anna, B.,
 1363 Fahlbusch, B., Foley, S., Fomba, K. W., George, C., Gnauk, T., Henning, S., Lee, T.,
 1364 Mertes, S., Roth, A., Stratmann, F., Borrmann, S., Hoppe, P., and Herrmann, H.: In-
 1365 cloud sulfate addition to single particles resolved with sulfur isotope analysis during
 1366 HCCT-2010, *Atmospheric Chemistry and Physics*, 14, 4219-4235, 10.5194/acp-14-
 1367 4219-2014, 2014.

1368 Hayden, K. L., Macdonald, A. M., Gong, W., Toom-Sauntry, D., Anlauf, K. G., Leithead, A.,
 1369 Li, S. M., Leaitch, W. R., and Noone, K.: Cloud processing of nitrate, *J. Geophys.
 1370 Res.-Atmos.*, 113, D18201, 10.1029/2007jd009732, 2008.

1371 Healy, R., Evans, G., Murphy, M., Sierau, B., Arndt, J., McGillicuddy, E., O'Connor, I.,
 1372 Sodeau, J., and Wenger, J.: Single-particle speciation of alkylamines in ambient
 1373 aerosol at five European sites, *Anal. Bioanal. Chem.*, 1-11, 10.1007/s00216-014-8092-
 1374 1, 2014a.

1375 Healy, R. M., Evans, G. J., Murphy, M., Jurányi, Z., Tritscher, T., Laborde, M., Weingartner,
 1376 E., Gysel, M., Poulain, L., Kamilli, K. A., Wiedensohler, A., O'Connor, I. P.,
 1377 McGillicuddy, E., Sodeau, J. R., and Wenger, J. C.: Predicting hygroscopic growth
 1378 using single particle chemical composition estimates, *Journal of Geophysical
 1379 Research: Atmospheres*, 119, 9567-9577, 10.1002/2014JD021888, 2014b.

1380 Henning, S., Wex, H., Hennig, T., Kiselev, A., Snider, J. R., Rose, D., Dusek, U., Frank, G.
 1381 P., Poschl, U., Kristensson, A., Bilde, M., Tillmann, R., Kiendler-Scharr, A., Mentel,
 1382 T. F., Walter, S., Schneider, J., Wennrich, C., and Stratmann, F.: Soluble mass,
 1383 hygroscopic growth, and droplet activation of coated soot particles during LACIS
 1384 Experiment in November (LExNo), *J. Geophys. Res.-Atmos.*, 115,
 1385 10.1029/2009jd012626, 2010.

1386 Henning, S., Dieckmann, K., Ignatius, K., Schäfer, M., Zedler, P., Harris, E., Sinha, B., van
 1387 Pinxteren, D., Mertes, S., Birmili, W., Merkel, M., Wu, Z., Wiedensohler, A., Wex,
 1388 H., Herrmann, H., and Stratmann, F.: Influence of cloud processing on CCN activation
 1389 behaviour in the Thuringian Forest, Germany during HCCT-2010, *Atmos. Chem.
 1390 Phys.*, 14, 7859-7868, 10.5194/acp-14-7859-2014, 2014.

1391 Herrmann, H., Wolke, R., Muller, K., Bruggemann, E., Gnauk, T., Barzaghi, P., Mertes, S.,
 1392 Lehmann, K., Massling, A., Birmili, W., Wiedensohler, A., Wierprecht, W., Acker,
 1393 K., Jaeschke, W., Kramberger, H., Svrčina, B., Bachmann, K., Collett, J. L., Galgon,
 1394 D., Schwirn, K., Nowak, A., van Pinxteren, D., Plewka, A., Chemnitzer, R., Rud, C.,
 1395 Hofmann, D., Tilgner, A., Diehl, K., Heinold, B., Hinneburg, D., Knoth, O., Sehili, A.
 1396 M., Simmel, M., Wurzler, S., Majdik, Z., Mauersberger, G., and Muller, F.: FEBUKO

1397 and MODMEP: Field measurements and modelling of aerosol and cloud multiphase
1398 processes, *Atmos. Environ.*, 39, 4169-4183, 10.1016/j.atmosenv.2005.02.004, 2005.

1399 Hinz, K. P., Greweling, M., Drews, F., and Spengler, B.: Data processing in on-line laser
1400 mass spectrometry of inorganic, organic, or biological airborne particles, *Journal of*
1401 *the American Society for Mass Spectrometry*, 10, 648-660, 10.1016/s1044-
1402 0305(99)00028-8, 1999.

1403 Hinz, K. P., Erdmann, N., Gruning, C., and Spengler, B.: Comparative parallel
1404 characterization of particle populations with two mass spectrometric systems
1405 LAMPAS 2 and SPASS, *Int. J. Mass Spectrom.*, 258, 151-166,
1406 10.1016/j.ijms.2006.09.008, 2006.

1407 Hinz, K. P., and Spengler, B.: Instrumentation, data evaluation and quantification in on-line
1408 aerosol mass spectrometry, *J. Mass Spectrom.*, 42, 843-860, 2007.

1409 Hitzenberger, R., Berner, A., Kromp, R., Kasper-Giebl, A., Limbeck, A., Tschewenka, W.,
1410 and Puxbaum, H.: Black carbon and other species at a high-elevation European site
1411 (Mount Sonnblick, 3106 m, Austria): Concentrations and scavenging efficiencies, *J.*
1412 *Geophys. Res.-Atmos.*, 105, 24637-24645, 10.1029/2000jd900349, 2000.

1413 Jacobson, M. Z.: Strong radiative heating due to the mixing state of black carbon in
1414 atmospheric aerosols, *Nature*, 409, 695-697, 10.1038/35055518, 2001.

1415 Jeong, C. H., McGuire, M. L., Godri, K. J., Slowik, J. G., Rehbein, P. J. G., and Evans, G. J.:
1416 Quantification of aerosol chemical composition using continuous single particle
1417 measurements, *Atmospheric Chemistry and Physics*, 11, 7027-7044, 10.5194/acp-11-
1418 7027-2011, 2011.

1419 Kamphus, M., Ettner-Mahl, M., Klimach, T., Drewnick, F., Keller, L., Cziczo, D. J., Mertes,
1420 S., Borrmann, S., and Curtius, J.: Chemical composition of ambient aerosol, ice
1421 residues and cloud droplet residues in mixed-phase clouds: single particle analysis
1422 during the Cloud and Aerosol Characterization Experiment (CLACE 6), *Atmospheric*
1423 *Chemistry and Physics*, 10, 8077-8095, 10.5194/acp-10-8077-2010, 2010.

1424 Klimach, T.: Chemische Zusammensetzung der Aerosole: Design und Datenauswertung eines
1425 Einzelpartikel-Laserablationsmassenspektrometers, Johannes Gutenberg-Universität,
1426 Mainz, 2012.

1427 Koehler, K. A., DeMott, P. J., Kreidenweis, S. M., Popovicheva, O. B., Petters, M. D.,
1428 Carrico, C. M., Kireeva, E. D., Khokhlova, T. D., and Shonija, N. K.: Cloud
1429 condensation nuclei and ice nucleation activity of hydrophobic and hydrophilic soot
1430 particles, *Physical Chemistry Chemical Physics*, 11, 7906-7920, Doi
1431 10.1039/B905334b, 2009.

1432 Korn, M. D. A., dos Santos, D. S. S., Welz, B., Vale, M. G. R., Teixeira, A. P., Lima, D. D.,
1433 and Ferreira, S. L. C.: Atomic spectrometric methods for the determination of metals
1434 and metalloids in automotive fuels - A review, *Talanta*, 73, 1-11,
1435 10.1016/j.talanta.2007.03.036, 2007.

1436 Laj, P., Fuzzi, S., Facchini, M. C., Lind, J. A., Orsi, G., Preiss, M., Maser, R., Jaeschke, W.,
1437 Seyffer, E., Helas, G., Acker, K., Wieprecht, W., Moller, D., Arends, B. G., Mols, J.
1438 J., Colvile, R. N., Gallagher, M. W., Beswick, K. M., Hargreaves, K. J., StoretonWest,
1439 R. L., and Sutton, M. A.: Cloud processing of soluble gases, *Atmos. Environ.*, 31,
1440 2589-2598, 10.1016/s1352-2310(97)00040-x, 1997a.

1441 Laj, P., Fuzzi, S., Facchini, M. C., Orsi, G., Berner, A., Kruisz, C., Wobrock, W., Hallberg,
1442 A., Bower, K. N., Gallagher, M. W., Beswick, K. M., Colvile, R. N., Choulaton, T.
1443 W., Nason, P., and Jones, B.: Experimental evidence for in-cloud production of
1444 aerosol sulphate, *Atmos. Environ.*, 31, 2503-2514, [http://dx.doi.org/10.1016/S1352-
1445 2310\(96\)00217-8](http://dx.doi.org/10.1016/S1352-2310(96)00217-8), 1997b.

1446 Lanz, V. A., Prévôt, A. S. H., Alfarra, M. R., Weimer, S., Mohr, C., DeCarlo, P. F., Gianini,
 1447 M. F. D., Hueglin, C., Schneider, J., Favez, O., D'Anna, B., George, C., and
 1448 Baltensperger, U.: Characterization of aerosol chemical composition with aerosol
 1449 mass spectrometry in Central Europe: an overview, *Atmospheric Chemistry and*
 1450 *Physics*, 10, 10453-10471, 10.5194/acp-10-10453-2010, 2010.
 1451 Limbeck, A., and Puxbaum, H.: Dependence of in-cloud scavenging of polar organic aerosol
 1452 compounds on the water solubility, *J. Geophys. Res.-Atmos.*, 105, 19857-19867,
 1453 10.1029/2000jd900123, 2000.
 1454 Liu, P., Ziemann, P. J., Kittelson, D. B., and McMurry, P. H.: Generating particle beams of
 1455 controlled dimensions and divergence: 1. Theory of particle motion in aerodynamic
 1456 lenses and nozzle expansions, *Aerosol Sci. Technol.*, 22, 293-313, 1995a.
 1457 Liu, P., Ziemann, P. J., Kittelson, D. B., and McMurry, P. H.: Generating particle beams of
 1458 controlled dimensions and divergence: 2. Experimental evaluation of particle motion
 1459 in aerodynamic lenses and nozzle expansions, *Aerosol Sci. Technol.*, 22, 314-324,
 1460 1995b.
 1461 McFiggans, G., Artaxo, P., Baltensperger, U., Coe, H., Facchini, M. C., Feingold, G., Fuzzi,
 1462 S., Gysel, M., Laaksonen, A., Lohmann, U., Mentel, T. F., Murphy, D. M., O'Dowd,
 1463 C. D., Snider, J. R., and Weingartner, E.: The effect of physical and chemical aerosol
 1464 properties on warm cloud droplet activation, *Atmospheric Chemistry and Physics*, 6,
 1465 2593-2649, 2006.
 1466 Mertes, S., Galgon, D., Schwirn, K., Nowak, A., Lehmann, K., Massling, A., Wiedensohler,
 1467 A., and Wieprecht, W.: Evolution of particle concentration and size distribution
 1468 observed upwind, inside and downwind hill cap clouds at connected flow conditions
 1469 during FEBUKO, *Atmos. Environ.*, 39, 4233-4245, 10.1016/j.atmosenv.2005.02.009,
 1470 2005a.
 1471 Mertes, S., Lehmann, K., Nowak, A., Massling, A., and Wiedensohler, A.: Link between
 1472 aerosol hygroscopic growth and droplet activation observed for hill-capped clouds at
 1473 connected flow conditions during FEBUKO, *Atmos. Environ.*, 39, 4247-4256,
 1474 10.1016/j.atmosenv.2005.02.010, 2005b.
 1475 Middlebrook, A. M., Murphy, D. M., Lee, S.-H., Thomson, D. S., Prather, K. A., Wenzel, R.
 1476 J., Liu, D.-Y., Phares, D. J., Rhoads, K. P., Wexler, A. S., Johnston, M. V., Jimenez, J.
 1477 L., Jayne, J. T., Worsnop, D. R., Yourshaw, I., Seinfeld, J. H., and Flagan, R. C.: A
 1478 comparison of particle mass spectrometers during the 1999 Atlanta Supersite Project,
 1479 *Journal of Geophysical Research: Atmospheres*, 108, 8424, 10.1029/2001JD000660,
 1480 2003.
 1481 Moffet, R. C., and Prather, K. A.: In-situ measurements of the mixing state and optical
 1482 properties of soot with implications for radiative forcing estimates, *Proceedings of the*
 1483 *National Academy of Sciences of the United States of America*, 106, 11872-11877,
 1484 10.1073/pnas.0900040106, 2009.
 1485 Murphy, D. M., Middlebrook, A. M., and Warshawsky, M.: Cluster analysis of data from the
 1486 Particle Analysis by Laser Mass Spectrometry (PALMS) instrument, *Aerosol Sci.*
 1487 *Technol.*, 37, 382-391, 10.1080/02786820390125241, 2003.
 1488 Ogren, J. A., Heintzenberg, J., and Charlson, R. J.: Insitu sampling of clouds with a droplet to
 1489 aerosol converter, *Geophys. Res. Lett.*, 12, 121-124, 10.1029/GL012i003p00121,
 1490 1985.
 1491 Petzold, A., Ogren, J. A., Fiebig, M., Laj, P., Li, S. M., Baltensperger, U., Holzer-Popp, T.,
 1492 Kinne, S., Pappalardo, G., Sugimoto, N., Wehrli, C., Wiedensohler, A., and Zhang, X.
 1493 Y.: Recommendations for reporting "black carbon" measurements, *Atmospheric*
 1494 *Chemistry and Physics*, 13, 8365-8379, 10.5194/acp-13-8365-2013, 2013.

1495 Posfai, M., Simonics, R., Li, J., Hobbs, P. V., and Buseck, P. R.: Individual aerosol particles
1496 from biomass burning in southern Africa: 1. Compositions and size distributions of
1497 carbonaceous particles, *J. Geophys. Res.-Atmos.*, 108, 10.1029/2002jd002291, 2003.

1498 Pratt, K. A., Hatch, L. E., and Prather, K. A.: Seasonal Volatility Dependence of Ambient
1499 Particle Phase Amines, *Environ. Sci. Technol.*, 43, 5276-5281, 10.1021/es803189n,
1500 2009.

1501 Pratt, K. A., and Prather, K. A.: Aircraft measurements of vertical profiles of aerosol mixing
1502 states, *J. Geophys. Res.-Atmos.*, 115, 10, D11305, 10.1029/2009jd013150, 2010.

1503 Pratt, K. A., Twohy, C. H., Murphy, S. M., Moffet, R. C., Heymsfield, A. J., Gaston, C. J.,
1504 DeMott, P. J., Field, P. R., Henn, T. R., Rogers, D. C., Gilles, M. K., Seinfeld, J. H.,
1505 and Prather, K. A.: Observation of playa salts as nuclei in orographic wave clouds, *J.*
1506 *Geophys. Res.-Atmos.*, 115, D15301, 10.1029/2009jd013606, 2010.

1507 Pratt, K. A., Murphy, S. M., Subramanian, R., DeMott, P. J., Kok, G. L., Campos, T., Rogers,
1508 D. C., Prenni, A. J., Heymsfield, A. J., Seinfeld, J. H., and Prather, K. A.: Flight-based
1509 chemical characterization of biomass burning aerosols within two prescribed burn
1510 smoke plumes, *Atmospheric Chemistry and Physics*, 11, 12549-12565, 10.5194/acp-
1511 11-12549-2011, 2011.

1512 Rehbein, P. J. G., Jeong, C. H., McGuire, M. L., Yao, X. H., Corbin, J. C., and Evans, G. J.:
1513 Cloud and Fog Processing Enhanced Gas-to-Particle Partitioning of Trimethylamine,
1514 *Environ. Sci. Technol.*, 45, 4346-4352, 10.1021/es1042113, 2011.

1515 Ross, K. E., Piketh, S. J., Brientjes, R. T., Burger, R. P., Swap, R. J., and Annegarn, H. J.:
1516 Spatial and seasonal variations in CCN distribution and the aerosol-CCN relationship
1517 over southern Africa, *J. Geophys. Res.-Atmos.*, 108, 10.1029/2002jd002384, 2003.

1518 Roth, A.: Untersuchungen von Aerosolpartikeln und Wolkenresidualpartikeln mittels
1519 Einzelpartikel-Massenspektrometrie und optischen Methoden, PhD Thesis (in
1520 German), University Mainz, 178 pp., <http://d-nb.info/1053202164/34>, 2014.

1521 Schade, G. W., and Crutzen, P. J.: Emission of aliphatic-amines from animal husbandry and
1522 their reactions - potential source of N₂O and HCN, *J. Atmos. Chem.*, 22, 319-346,
1523 10.1007/bf00696641, 1995.

1524 Schneider, J., Weimer, S., Drewnick, F., Borrmann, S., Helas, G., Gwaze, P., Schmid, O.,
1525 Andreae, M. O., and Kirchner, U.: Mass spectrometric analysis and aerodynamic
1526 properties of various types of combustion-related aerosol particles, *Int. J. Mass*
1527 *Spectrom.*, 258, 37-49, 2006.

1528 Schneider, J., Mertes, S., Van Pinxteren, D., Herrmann, H., and Borrmann, S.: In-situ mass
1529 spectrometric analysis of cloud residuals and interstitial aerosol composition on
1530 orographic clouds during HCCT-2010: Uptake of nitric acid in cloud droplets,
1531 *Atmospheric Chemistry and Physics*, in preparation, 2015.

1532 Sedlak, D. L., Hoigne, J., David, M. M., Colvile, R. N., Seyffer, E., Acker, K., Wiepercht, W.,
1533 Lind, J. A., and Fuzzi, S.: The cloudwater chemistry of iron and copper at Great Dun
1534 Fell, UK, *Atmos. Environ.*, 31, 2515-2526, 10.1016/s1352-2310(96)00080-5, 1997.

1535 Sellegri, K., Laj, P., Dupuy, R., Legrand, M., Preunkert, S., and Putaud, J. P.: Size-dependent
1536 scavenging efficiencies of multicomponent atmospheric aerosols in clouds, *J.*
1537 *Geophys. Res.-Atmos.*, 108, 4334, 10.1029/2002jd002749, 2003.

1538 Sellegri, K., Umann, B., Hanke, M., and Arnold, F.: Deployment of a ground-based CIMS
1539 apparatus for the detection of organic gases in the boreal forest during the QUEST
1540 campaign, *Atmospheric Chemistry and Physics*, 5, 357-372, 2005.

1541 Shields, L. G., Suess, D. T., and Prather, K. A.: Determination of single particle mass spectral
1542 signatures from heavy-duty diesel vehicle emissions for PM_{2.5} source apportionment,
1543 *Atmos. Environ.*, 41, 3841-3852, 10.1016/j.atmosenv.2007.01.025, 2007.

- 1544 Silva, P. J., Liu, D. Y., Noble, C. A., and Prather, K. A.: Size and chemical characterization of
 1545 individual particles resulting from biomass burning of local Southern California
 1546 species, *Environ. Sci. Technol.*, 33, 3068-3076, 10.1021/es980544p, 1999.
- 1547 Silva, P. J., and Prather, K. A.: Interpretation of mass spectra from organic compounds in
 1548 aerosol time-of-flight mass spectrometry, *Anal. Chem.*, 72, 3553-3562, 2000.
- 1549 Silva, P. J., Carlin, R. A., and Prather, K. A.: Single particle analysis of suspended soil dust
 1550 from Southern California, *Atmos. Environ.*, 34, 1811-1820, 10.1016/s1352-
 1551 2310(99)00338-6, 2000.
- 1552 Simoneit, B. R. T., Schauer, J. J., Nolte, C. G., Oros, D. R., Elias, V. O., Fraser, M. P., Rogge,
 1553 W. F., and Cass, G. R.: Levoglucosan, a tracer for cellulose in biomass burning and
 1554 atmospheric particles, *Atmos. Environ.*, 33, 173-182, 1999.
- 1555 Snyder, D. C., Schauer, J. J., Gross, D. S., and Turner, J. R.: Estimating the contribution of
 1556 point sources to atmospheric metals using single-particle mass spectrometry, *Atmos.*
 1557 *Environ.*, 43, 4033-4042, 10.1016/j.atmosenv.2009.05.011, 2009.
- 1558 Sodeman, D. A., Toner, S. M., and Prather, K. A.: Determination of single particle mass
 1559 spectral signatures from light-duty vehicle emissions, *Environ. Sci. Technol.*, 39,
 1560 4569-4580, 10.1021/es0489947, 2005.
- 1561 Tilgner, A., Majdik, Z., Sehili, A. M., Simmel, M., Wolke, R., and Herrmann, H.: SPACCIM:
 1562 Simulations of the multiphase chemistry occurring in the FEBUKO hill cap cloud
 1563 experiments, *Atmos. Environ.*, 39, 4389-4401, 10.1016/j.atmosenv.2005.02.028, 2005.
- 1564 Tilgner, A., Schöne, L., Bräuer, P., van Pinxteren, D., Hoffmann, E., Spindler, G., Styler, S.
 1565 A., Mertes, S., Birmili, W., Otto, R., Merkel, M., Weinhold, K., Wiedensohler, A.,
 1566 Deneke, H., Schrödner, R., Wolke, R., Schneider, J., Haunold, W., Engel, A., Wéber,
 1567 A., and Herrmann, H.: Comprehensive assessment of meteorological conditions and
 1568 airflow connectivity during HCCT-2010, *Atmos. Chem. Phys.*, 14, 9105-9128,
 1569 10.5194/acp-14-9105-2014, 2014.
- 1570 Tolocka, M. P., Lake, D. A., Johnston, M. V., and Wexler, A. S.: Number concentrations of
 1571 fine and ultrafine particles containing metals, *Atmos. Environ.*, 38, 3263-3273,
 1572 10.1016/j.atmosenv.2004.03.010, 2004.
- 1573 Trimborn, A., Hinz, K. P., and Spengler, B.: Online analysis of atmospheric particles with a
 1574 transportable laser mass spectrometer during LACE 98, *J. Geophys. Res.*, 107, LAC
 1575 13-11 - LAC 13-10, 2002.
- 1576 van Pinxteren, M., Fiedler, B., van Pinxteren, D., Iinuma, Y., Körtzinger, A., and Herrmann,
 1577 H.: Chemical characterization of sub-micrometer aerosol particles in the tropical
 1578 Atlantic Ocean: marine and biomass burning influences, Submitted to *Atmospheric*
 1579 *Chemistry and Physics*, 2015.
- 1580 Vogt, R., Kirchner, U., Scheer, V., Hinz, K. P., Trimborn, A., and Spengler, B.: Identification
 1581 of diesel exhaust particles at an Autobahn, urban and rural location using single-
 1582 particle mass spectrometry, *J. Aerosol. Sci.*, 34, 319-337, 10.1016/s0021-
 1583 8502(02)00179-9, 2003.
- 1584 Weimer, S.: Particle emission traffic and wood combustion and its impact on spatial
 1585 distributions of submicron particulate matter, PhD thesis, Eidgenössische Technische
 1586 Hochschule Zürich, 2008.
- 1587 Wendisch, M., and Brenguier, J.-L.: *Airborne Measurements for Environmental Research:
 1588 Methods and Instruments*, Wiley-VCH Verlag GmbH & Co. KGaA, Weinheim, 2013.
- 1589 Wobrock, W., Schell, D., Maser, R., Jaeschke, W., Georgii, H. W., Wiedensohler, W., Arends, B.
 1590 G., Mols, J. J., Kos, G. P. A., Fuzzi, S., Facchini, M. C., Orsi, G., Berner, A., Solly, I.,
 1591 Kruisz, C., Svenningsson, I. B., Wiedensohler, A., Hansson, H. C., Ogren, J. A.,
 1592 Noone, K. J., Hallberg, A., Pahl, S., Schneider, T., Winkler, P., Winiwarter, W.,

1593 Colvile, R. N., Choularton, T. W., Flossmann, A. I., and Borrmann, S.: The Kleiner
1594 Feldberg Cloud Experiment 1990. An overview, *J. Atmos. Chem.*, 19, 3-35,
1595 10.1007/BF00696581, 1994.

1596 Zelenyuk, A., Imre, D., Cai, Y., Mueller, K., Han, Y. P., and Imrich, P.: SpectraMiner, an
1597 interactive data mining and visualization software for single particle mass
1598 spectroscopy: A laboratory test case, *Int. J. Mass Spectrom.*, 258, 58-73,
1599 10.1016/j.ijms.2006.06.015, 2006.

1600 Zelenyuk, A., Imre, D., Nam, E. J., Han, Y. P., and Mueller, K.: ClusterSculptor: Software for
1601 expert-steered classification of single particle mass spectra, *Int. J. Mass Spectrom.*,
1602 275, 1-10, 10.1016/j.ijms.2008.04.033, 2008.

1603 Zelenyuk, A., Imre, D., Earle, M., Easter, R., Korolev, A., Leaitch, R., Liu, P., Macdonald, A.
1604 M., Ovchinnikov, M., and Strapp, W.: In Situ Characterization of Cloud Condensation
1605 Nuclei, Interstitial, and Background Particles Using the Single Particle Mass
1606 Spectrometer, SPLAT II, *Anal. Chem.*, 82, 7943-7951, 10.1021/ac1013892, 2010.

1607 Zhang, G. H., Bi, X. H., Chan, L. Y., Li, L., Wang, X. M., Feng, J. L., Sheng, G. Y., Fu, J.
1608 M., Li, M., and Zhou, Z.: Enhanced trimethylamine-containing particles during fog
1609 events detected by single particle aerosol mass spectrometry in urban Guangzhou,
1610 China, *Atmos. Environ.*, 55, 121-126, 10.1016/j.atmosenv.2012.03.038, 2012.

1611 Zhao, W. X., Hopke, P. K., and Prather, K. A.: Comparison of two cluster analysis methods
1612 using single particle mass spectra, *Atmos. Environ.*, 42, 881-892,
1613 10.1016/j.atmosenv.2007.10.024, 2008.

1614

1615

1616 **Tables**

1617

1618 **Table 1.** Overview of the defined FCEs after Tilgner et al. (2014) during HCCT-2010 and the number of obtained single particle mass spectra
1619 by ALABAMA. FCE2.1, FCE4.1, FCE5.1 and FCE26.2 are statistically not significant.

Full cloud event	Start (CEST)	End (CEST)	Duration/ — in h	<u>Cloud information</u>	Number of mass spectra (cloud residues)
FCE1.1	14-09-2010 11:00	15-09-2010 01:50	14.8	<u>No pure orographic cloud, area covered by high clouds, stable stratification</u>	1351
FCE1.2	15-09-2010 03:00	15-09-2010 06:20	3.3	<u>Slight precipitation, slight stable thermal stratification</u>	128
FCE2.1	15-09-2010 23:00	16-09-2010 02:00	3	<u>No pure orographic cloud, no precipitation, stable stratification</u>	-
FCE4.1	16-09-2010 13:10	16-09-2010 15:00	1.8	<u>Slight precipitation, unstable thermal stratification</u>	5
FCE5.1	16-09-2010 21:40	16-09-2010 23:50	2.2	<u>No precipitation, slight stable stratification</u>	56
FCE7.1	24-09-2010 21:10	25-09-2010 00:50	3.7	<u>Stable thermal stratification, orographic cloud, no precipitation</u>	238
FCE11.2	01-10-2010 20:50	02-10-2010 03:10	6.3	<u>No precipitation, occlusion-related cloud</u>	117
FCE11.3	02-10-2010 07:10	03-10-2010 00:30	17.3	<u>Slight precipitation at beginning of event, partly orographic cloud, higher clouds occurred, stable thermal stratification</u>	974
FCE13.3	06-10-2010 06:50	07-10-2010 01:00	18.2	<u>Rather stable thermal stratification, orographic cloud</u>	1131
FCE22.0	19-10-2010	19-10-2010	7.2	<u>T < 0°C, rather stable thermal stratification, occlusion-related cloud</u>	1561

	01:50	09:00			
FCE22.1	19-10-2010 21:10	20-10-2010 02:30	5.3	<u>Slightly stable thermal stratification, lower stratiform cloudiness</u>	248
FCE24.0	21-10-2010 22:10	22-10-2010 10:00	11.8	<u>T < 0°C, quite stable thermal stratification, orographic cloud pattern, slight precipitation</u>	588
FCE26.1	23-10-2010 23:40	24-10-2010 07:20	7.7	<u>less stable thermal stratification, no pure orographic cloud, light precipitation</u>	356
FCE26.2	24-10-2010 08:40	24-10-2010 12:20	3.7	<u>Similar to FCE26.1, light postfrontal precipitation</u>	30

1620

1621 **Table 2.** Overview of particle types and the corresponding determined uncertainties of the
 1622 clustering by the fuzzy c-means algorithm. The particle types “mineral dust” and “Ca” were
 1623 not included in the reduced test data set.

Particle type	number MS	$\Delta_{\text{false positive}}$	$\Delta_{\text{false negative}}$	$\Delta_{\text{particle type}}$	$\Delta_{\text{particle type}} (\%)$
org, K	274	51	43	67	24
Org	162	21	1	21	13
amines	162	14	54	56	35
Soot	125	4	19	19	15
soot and org	120	12	35	37	31
diesel exhaust	18	8	3	9	50
biomass burning	223	14	36	39	17
K	106	31	8	32	30
sea salt	23	3	5	6	26
others	164	68	22	72	44

1624

1625

1626 **Table 3.** Overview of identified particle types and the characteristic peaks used for the assignment of clusters to a particle type. Additionally
 1627 the observed chemical composition of the particle types and the denotation used in the following (legend) are listed. Secondary inorganic
 1628 compounds like nitrate and sulphate were present in every particle type and have therefore not been used as characteristic signals for the
 1629 separation of particle types.

category	legend	method	characteristic signals	corresponding chemical composition
A	org, K	clustering	m/z 27 (C ₂ H ₃ ⁺), 39 (K ⁺), 43 (C ₃ H ₅ ⁺ /CH ₃ CO ⁺), 51(C ₄ H ₃ ⁺), organics, potassium, nitrate, sulfate 63 (C ₅ H ₃ ⁺), 77 (C ₆ H ₅ ⁺); m/z -59 (C ₃ H ₇ O ⁻ / C ₂ H ₃ O ₂ ⁻), -73 (C ₄ H ₉ O ⁻ /C ₃ H ₅ O ₂ ⁻) m/z 12 (C ⁺), 18 (NH ₄ ⁺), 27 (C ₂ H ₃ ⁺), 36 (C ₃ ⁺), 39 (K ⁺), 43 (C ₃ H ₅ ⁺ / CH ₃ CO ⁺), 48 (C ₄ ⁺)	organics, potassium, nitrate, sulfate
B	org	clustering	m/z 27 (C ₂ H ₃ ⁺), 43 (C ₃ H ₅ ⁺ / CH ₃ CO ⁺), C ₁₋₅ ⁺	organics, nitrate, sulfate
C	amines	clustering	m/z 18 (NH ₄ ⁺), 59 (N(CH ₃) ₃ ⁺)	amines, organics, nitrate, sulfate
D	soot	clustering	C _n ⁺ ; C _n ⁻	soot, nitrate, sulfate
E	soot and org	clustering	m/z 18 (NH ₄ ⁺), 27 (C ₂ H ₃ ⁺), 43 (C ₃ H ₅ ⁺ /CH ₃ CO ⁺), C _n ⁺ ; C _n ⁻	soot, organics, nitrate, sulfate
F	diesel exhaust	clustering	m/z 23 (Na ⁺), 40 (Ca ⁺), C _n ⁺ ; C _n ⁻	soot, sodium, calcium, nitrate
G	biomass burning	clustering	m/z 39 (K ⁺), C _n ⁺ ; C _n ⁻ m/z 23 (Na ⁺), 39 (K ⁺), 43 (C ₃ H ₅ ⁺ / CH ₃ CO ⁺), 51(C ₄ H ₃ ⁺), C _n ⁺ ; C _n ⁻ m/z 39 (K ⁺); m/z -26 (CN ⁻)	biomass burning, nitrate, sulfate
H	K	clustering	m/z 39 (K ⁺); m/z -46 (NO ₂ ⁻), -62 (NO ₃ ⁻), -97 (HSO ₄ ⁻)	potassium, nitrate, sulfate
I	sea salt	clustering	m/z 23 (Na ⁺), 39 (K ⁺); m/z -46 (NO ₂ ⁻), -62 (NO ₃ ⁻), -97 (HSO ₄ ⁻)	sodium, potassium, nitrate, sulfate (aged sea salt)
J	Ca	clustering	m/z 40 (Ca ⁺), 57 (CaOH ⁺)	calcium, soot, nitrate, sulfate
K	mineral dust	clustering & marker peak	m/z 56 (Fe ⁺)	Iron, sodium, potassium, calcium, nitrate, sulfate, phosphate
L	Fe, V	marker peak	m/z 56, m/z 51, m/z 67	vanadium, iron, nitrate, sulfate
N	Ni	marker peak	m/z 58	nickel, iron, vanadium, nitrate, sulfate
M	Pb	marker peak	m/z 208	lead, sodium, nitrate, sulfate
O	Others			

1630

1631 **Table 4.** Absolute and relative particle numbers detected by ALABAMA during the HCCT-
 1632 2010 campaign. The percentage of each particle type is subdivided into the fraction revealing
 1633 a diurnal trend and into the fraction without diurnal trend. All percentages refer to the total
 1634 number of 177752 analysed particles.

Particle type	Total number	Percentage	Number in clusters with diurnal trend	Percentage with diurnal trend	Number in clusters w/o diurnal trend	Percentage w/o diurnal trend
org, K	57163	32.2	27344	15.4	0	16.8
org	6295	3.54	6290	3.54	0	0.00281
amines	4910	2.76	4910	2.76	0	0
soot	25981	14.6	23546	13.2	0	1.37
soot, org	3931	2.21	2878	1.62	0	0.592
diesel exhaust	994	0.559	994	0.559	0	0
biomass burning	49873	28.1	37505	21.1	0	6.96
K	10052	5.66	9035	5.08	0	0.572
sea salt	1927	1.08	0	0	1927	1.08
others	13967	7.86	0	0	13967	7.86
Ca	263	0.148	0	0	263	0.148
mineral dust	756	0.425	0	0	756	0.425
Fe, V	569	0.242	0	0	569	0.32
Ni	641	0.361	0	0	641	0.361
Pb	430	0.242	0	0	430	0.242
Total	177752	100	112502	63.3	65250	36.7

1635

1636

1637 **Table 5.** Cloud and out-of-cloud periods (local time) used for the investigation of the particle
 1638 mixing state.

event	Out-of-cloud aerosol			cloud residues		
	start	end	mass spectra	start	end	mass spectra
I	15-09-2010 11:00	15-09-2010 23:30	1732	14-09-2010 11:00	15-09-2010 02:00	1351
II	21-10-2010 14:15	21-10-2010 22:15	1410	21-10-2010 23:24	22-10-2010 09:29	577

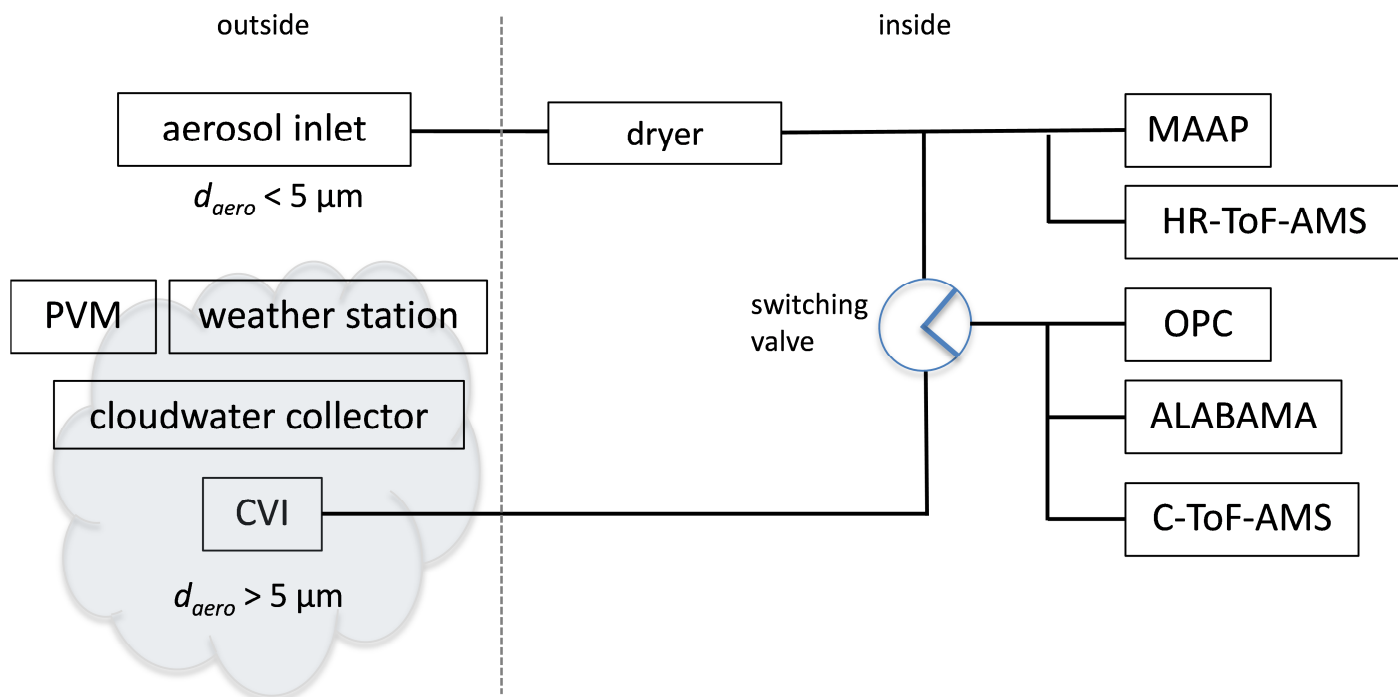
1639

1640

1641

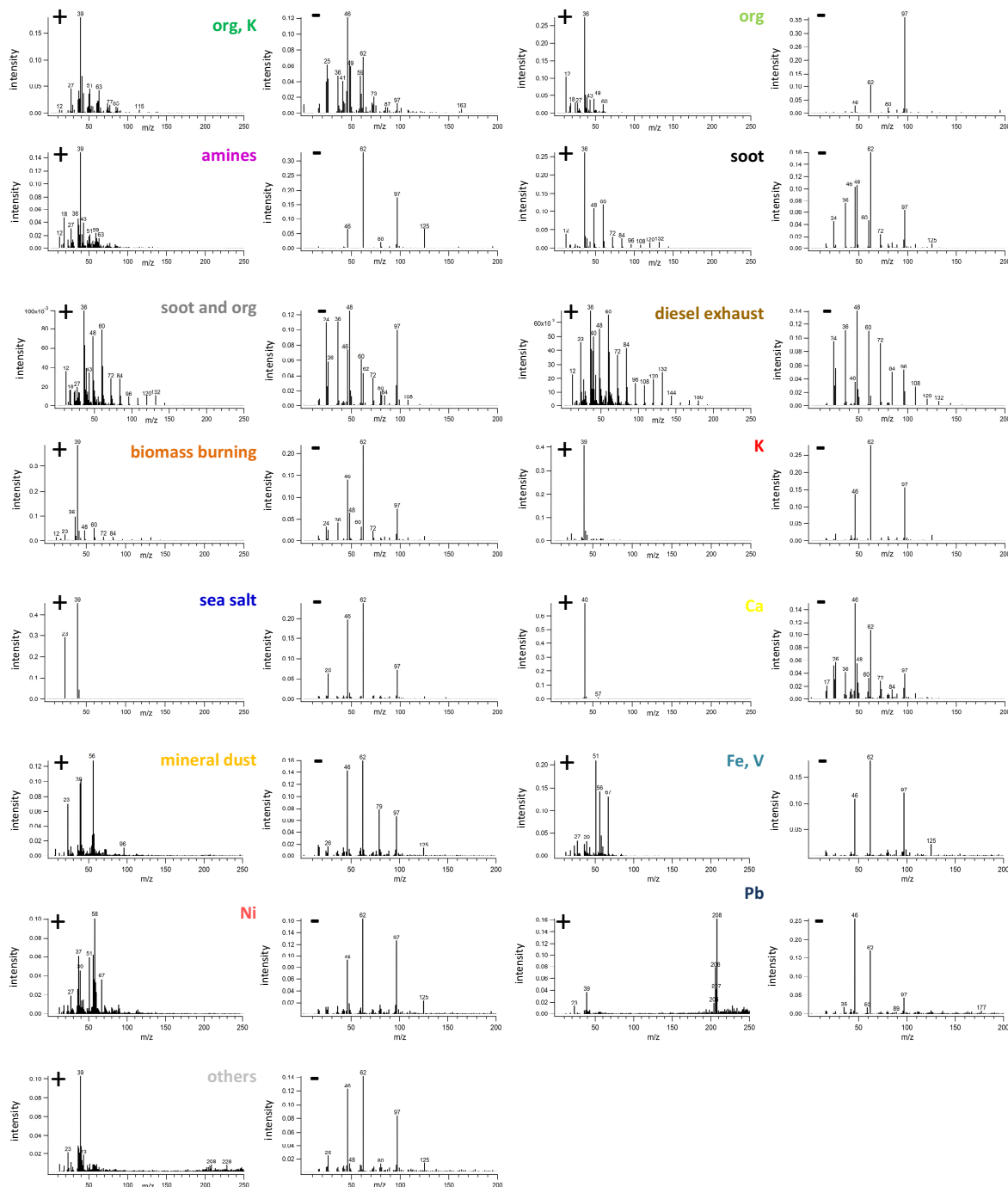
1642
1643
1644
1645
1646
1647

Figures



1648
1649
1650
1651
1652
1653
1654
1655

Figure 1. Measurement set-up and further operated instruments at the summit site Schmücke. Out-of-cloud aerosol was investigated by sampling through the aerosol inlet during cloud free periods while cloud residues were investigated by sampling through the CVI during cloud episodes.

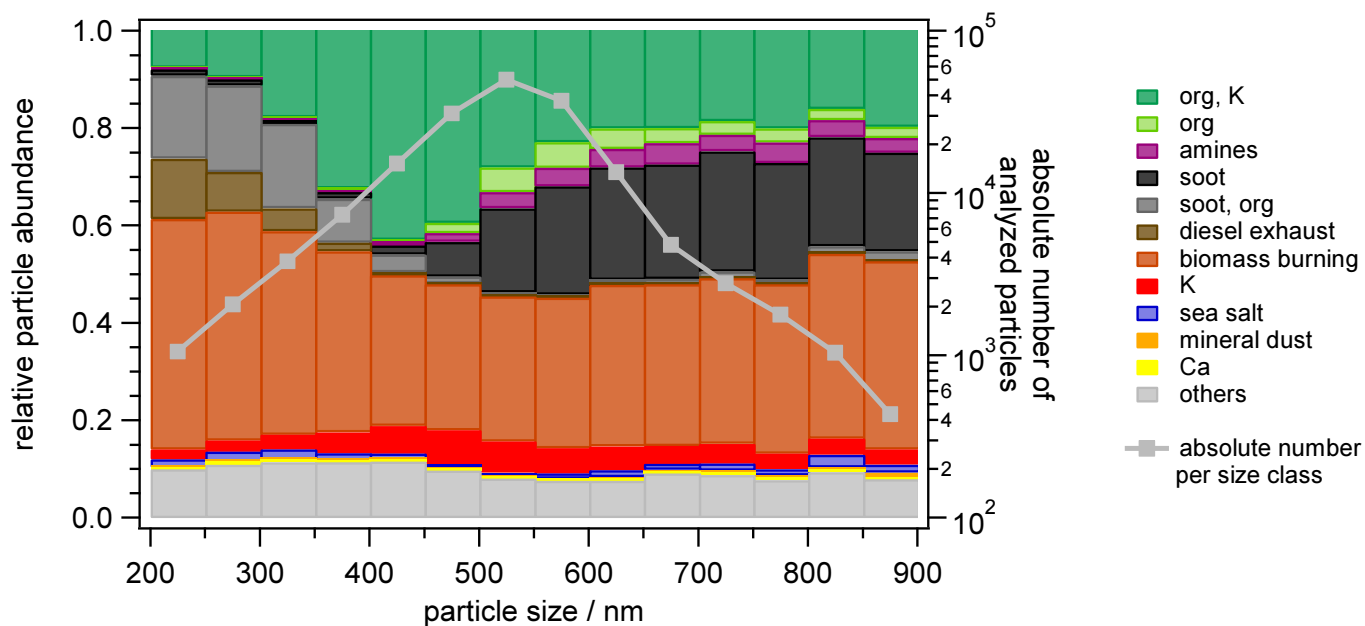


1657
1658

1659 **Figure 2.** Mean positive (left) and negative (right) mass spectra representative of the particle
 1660 types “org, K”, “org”, “amines”, “soot”, “soot and org”, “diesel exhaust”, “biomass burning”,
 1661 “K”, “sea salt” and “Ca”, “mineral dust”, “Fe,V”, “Ni”, “Pb” (with the separation of the Pb
 1662 isotopes clearly visible) and “others”.

1663

1664

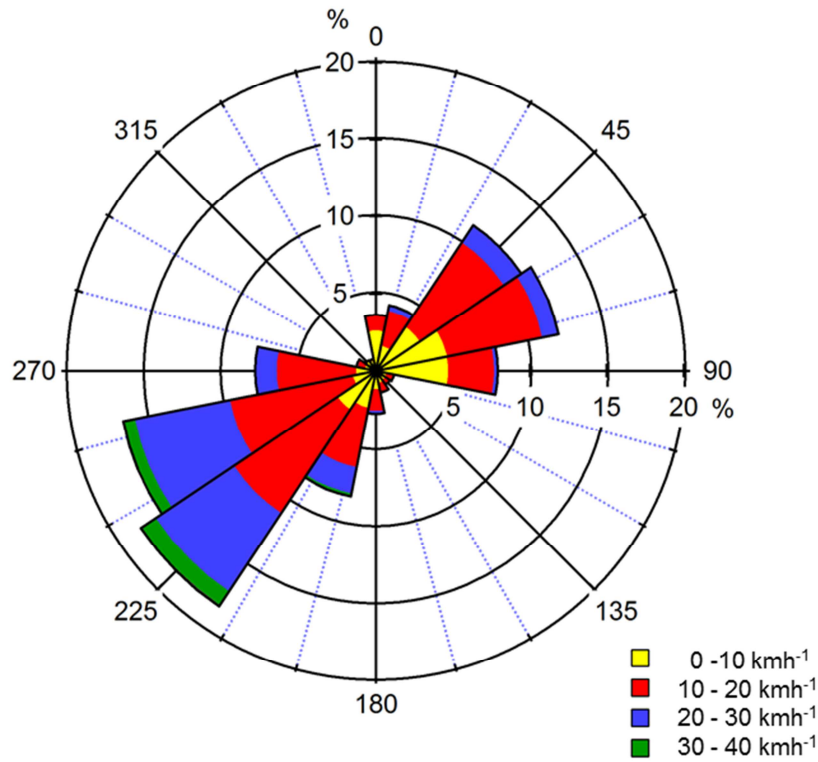


1665

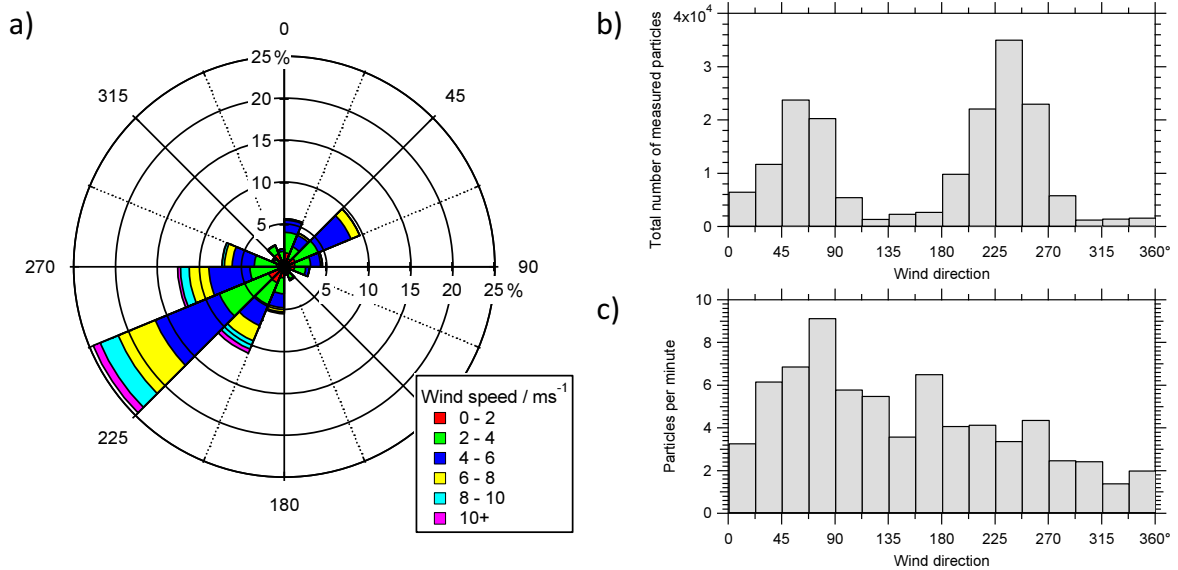
1666 **Figure 3.** Size resolved aerosol composition of the resulting particle types detected by the
1667 ALABAMA, binned into 50 nm size intervals. The absolute number of analysed particles per
1668 size class is given by the grey line.

1669

1670



1672



1673

1674

1675

1676

1677

1678

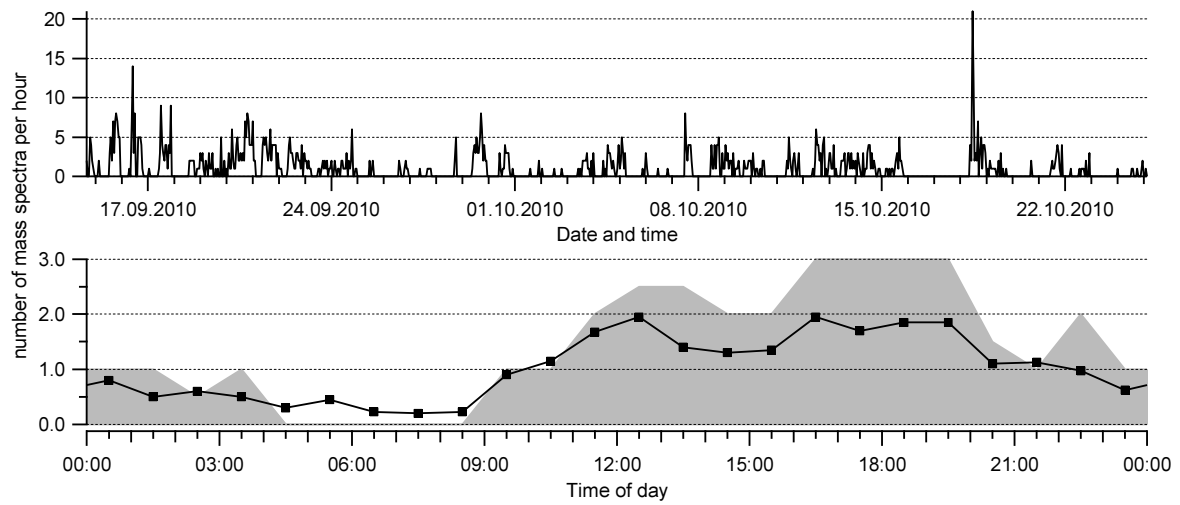
1679

Figure 4. a) Wind rose showing wind speed and direction for the whole time period. b) Absolute number of analyzed particles per wind direction. c) Same as b) but normalized to the measurement time per wind direction. Occurrence of wind directions and wind velocities based on the single particle mass spectra recording time. For example, for 18% of the detected mass spectra the wind direction was about 225°. Out of these, 10% showed a wind velocity of

1680 | ~~30–40 km h⁻¹, 45% of 20–30 km h⁻¹, 40% of 10–20 km h⁻¹ and 5% of 0–10 km h⁻¹. The~~
1681 | ~~percentages of the wind velocities correspond to the coloured area fraction of the pies.~~
1682
1683

1684

1685

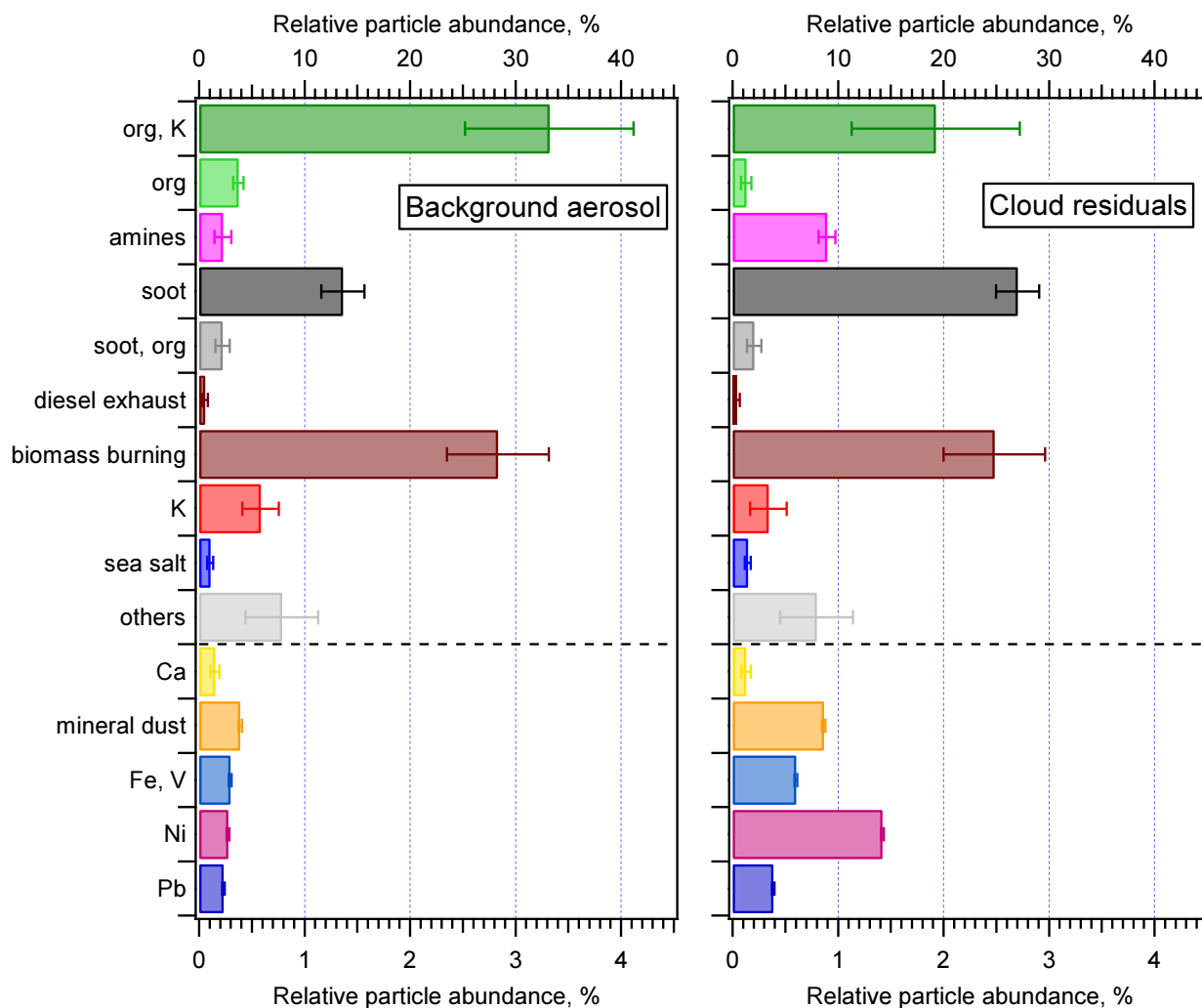


1686

1687

1688 **Figure 5.** Time series (top) and diurnal variations (bottom, LT) of the particle type “diesel
1689 exhaust” during HCCT-2010. Markers denote the mean values, the grey shaded area
1690 represents the upper quartile.

1691



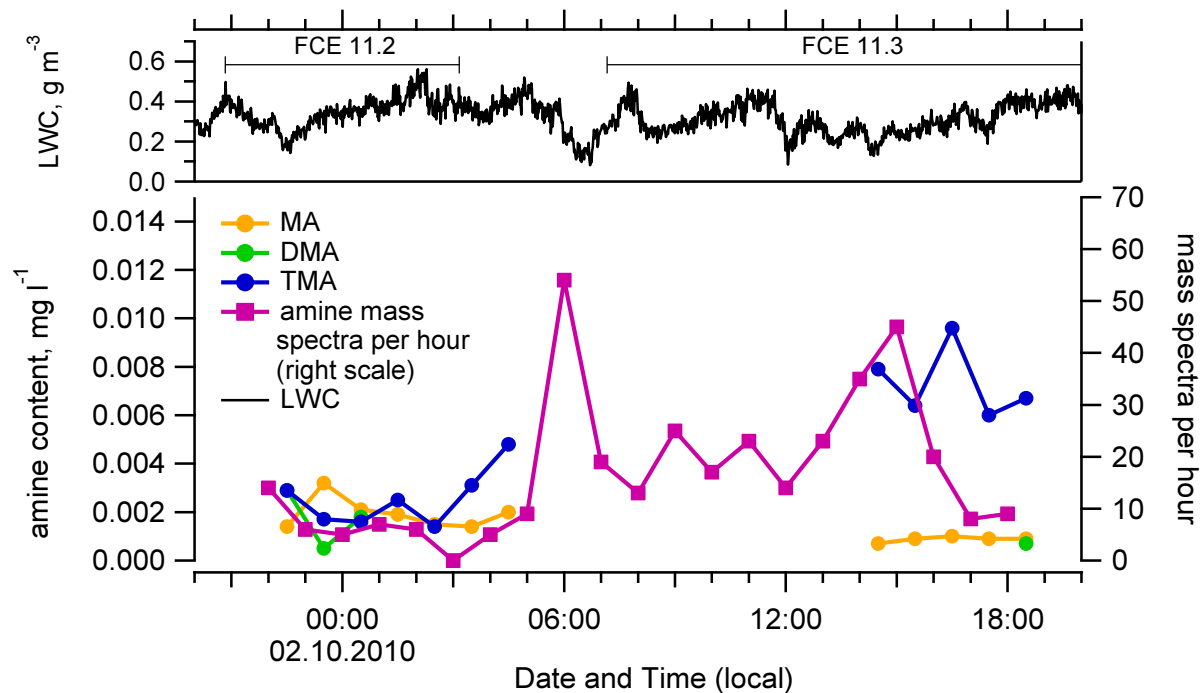
1693

1694 **Figure 6.** Aerosol composition of out-of-cloud aerosol (left) and cloud residual particles
 1695 (right) for the entire HCCT-2010 campaign. Uncertainties of the clustering were estimated
 1696 according to Section 2.4.2. In case of particle types determined by the marker peak method
 1697 (Section 2.4.3) uncertainties are based on Poisson statistic. Number of analysed particles: out-
 1698 of-cloud aerosol: 164595, cloud residues: 13157. Note that the scale is expanded by a factor
 1699 of 10 below the dashed line (bottom axis), particle abundances above the dashed line refer to
 1700 the top axis.

1701

1702

1703

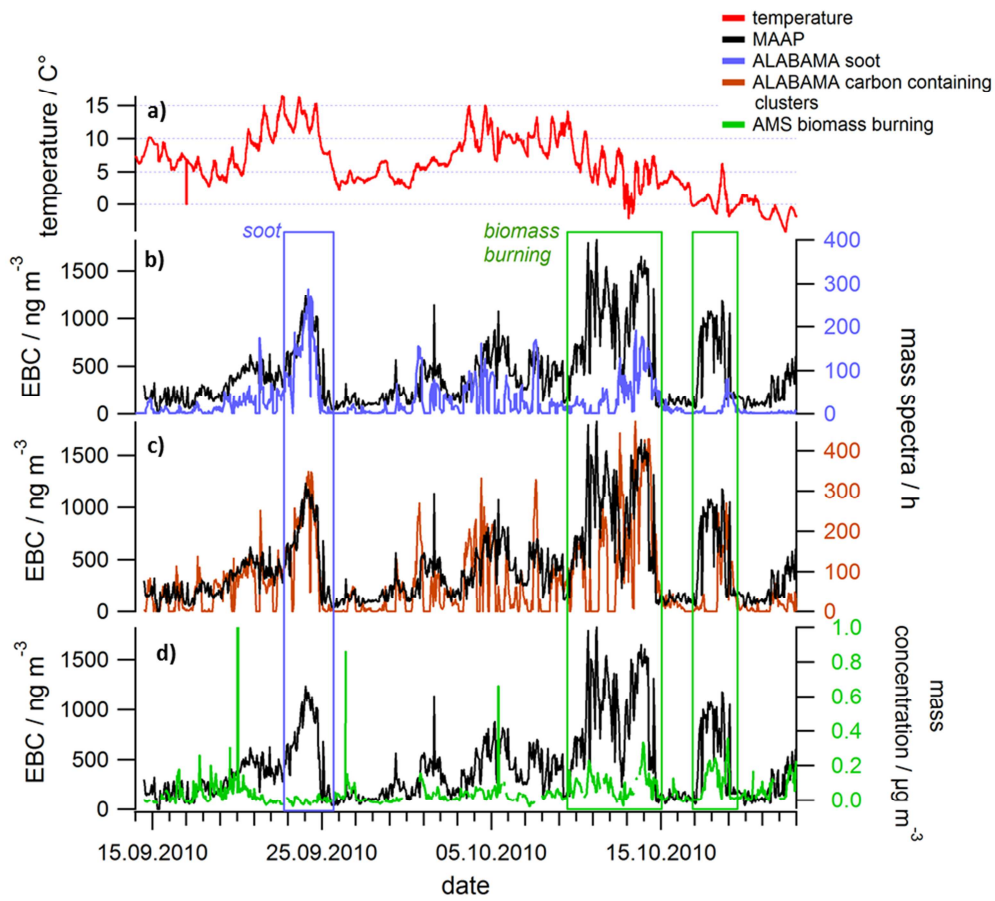


1704

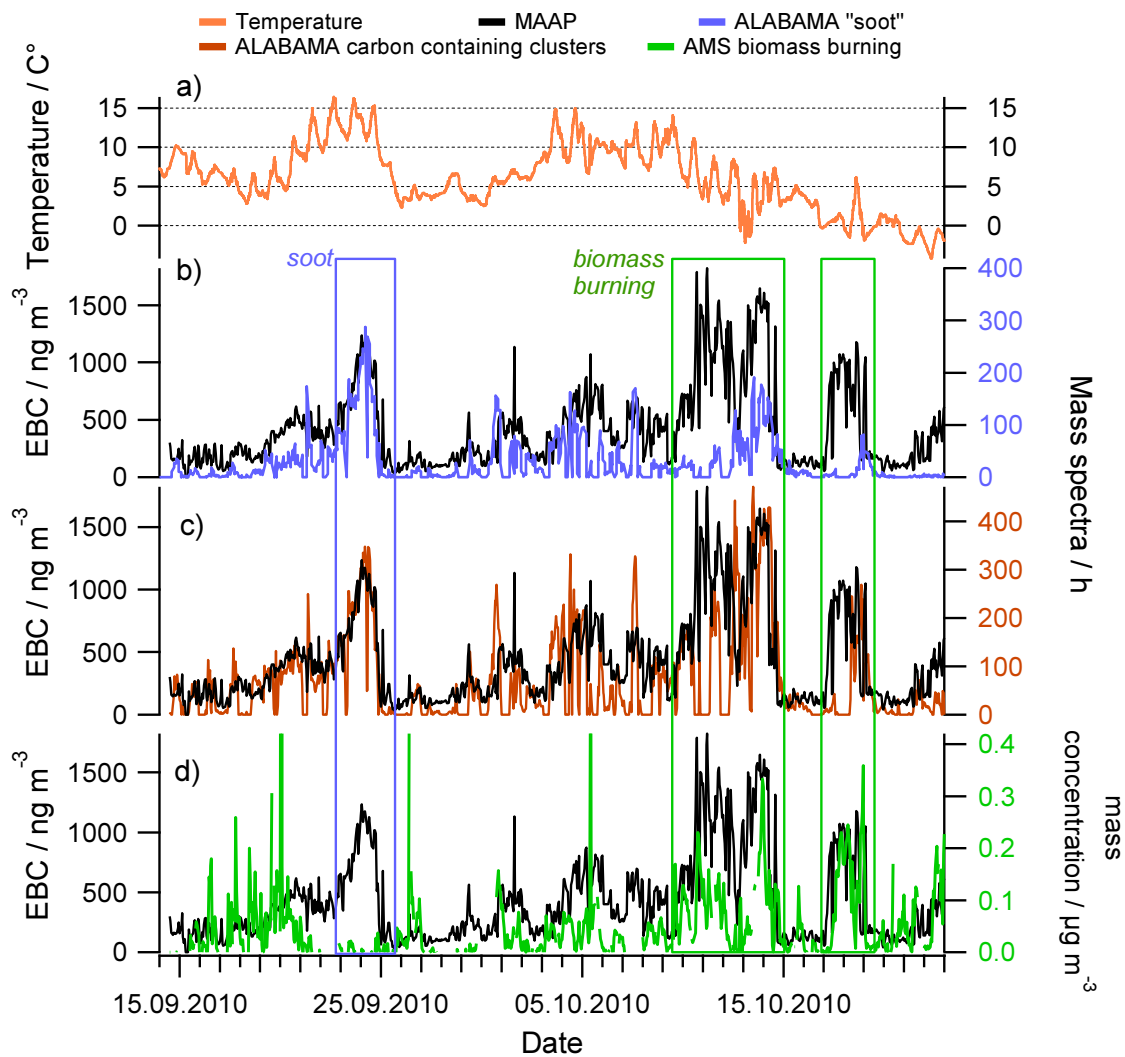
1705 **Figure 7.** Time series (LT) of the amine compounds methylamine (MA), dimethylamine
1706 (DMA) and trimethylamine (TMA) from cloud water samples on 02 October 2010 (FCE11.2
1707 and FCE 11.3) compared to the time series (number of mass spectra per hour) of amine-
1708 containing cloud residues. The upper panel shows the liquid water content (LWC) and the
1709 FCE times.

1710

1711



1713



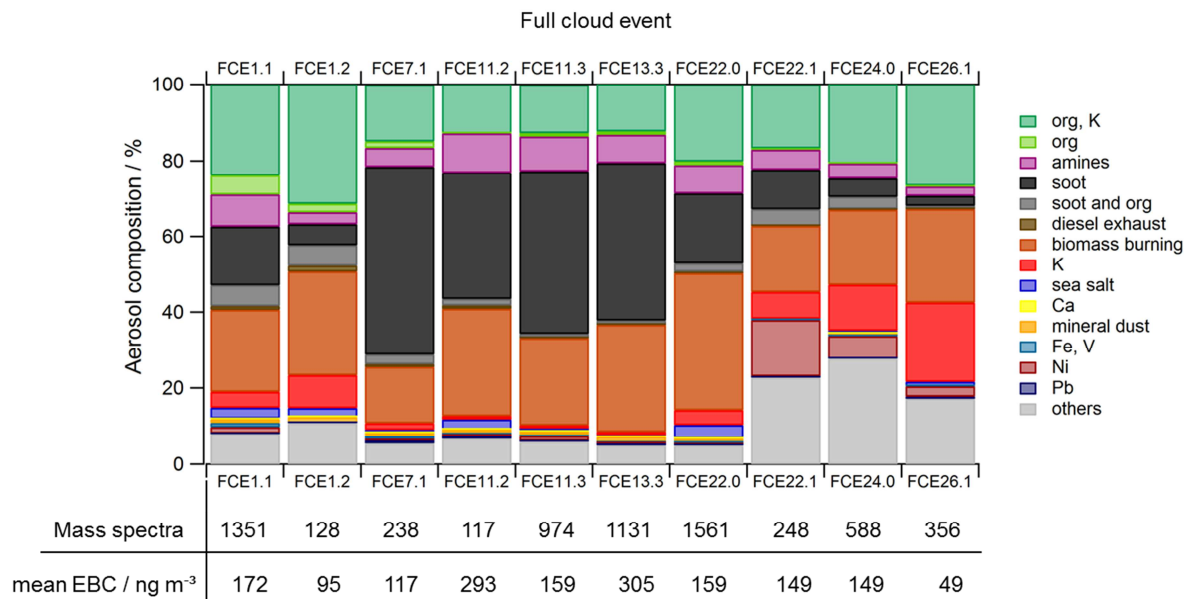
1714

1715 **Figure 8.** Time series (local time) of combustion related parameters observed during HCCT-
 1716 2010. (a) Temperature; (b) Equivalent black carbon (EBC) together with the particle type
 1717 "soot" (blue); (c) EBC along with the particle type biomass burning (brown); (d) EBC along
 1718 with the biomass burning aerosol inferred from AMS data (green).

1719

1720

1721



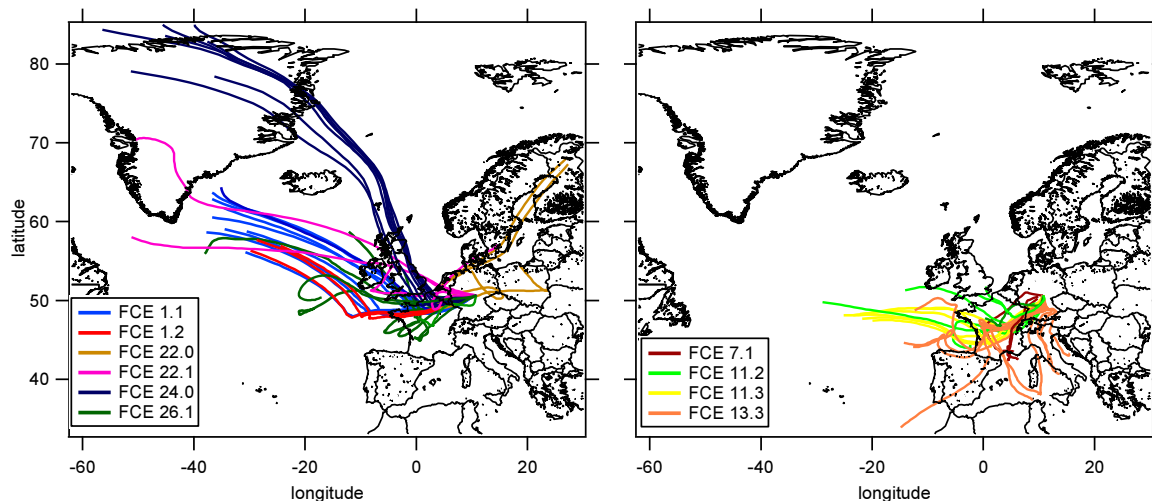
1722

1723 **Figure 9.** Cloud residue composition during full cloud events (FCE). The number of obtained
 1724 single particle mass spectra and the mean EBC concentration per event is given below the
 1725 graph. Only FCE with more than 100 mass spectra are included (see Table 1).

1726

1727

1728



1729

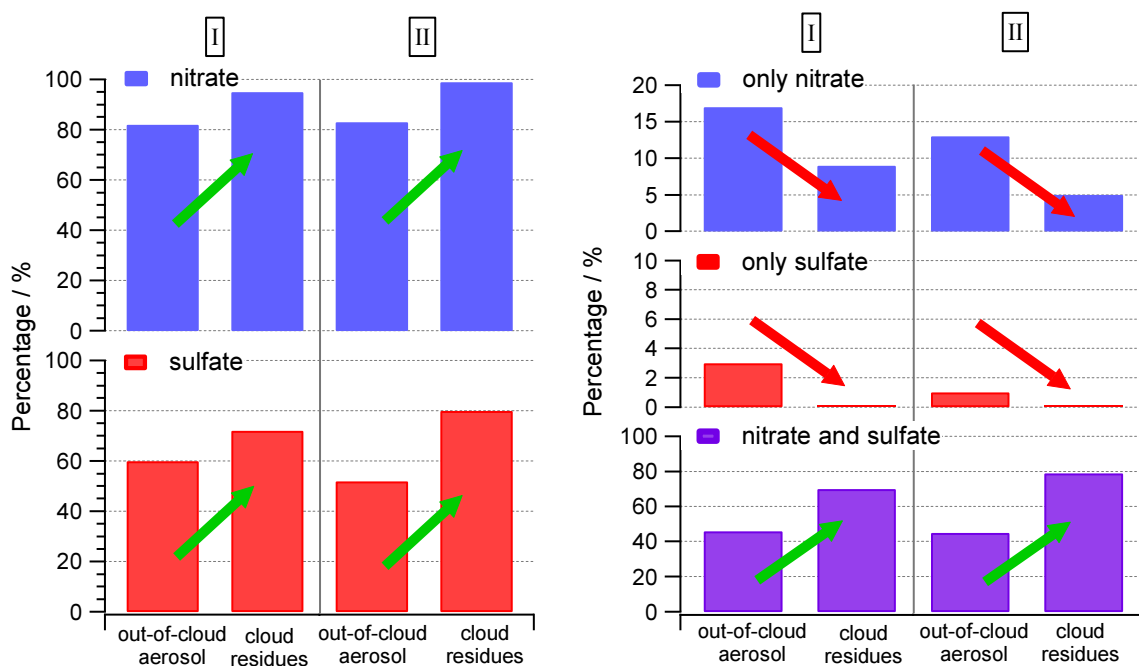
1730

1731 **Figure 10.** HYSPLIT back trajectories (96 hours) for air masses encountered during the FCE
1732 displayed in Figure 9. Left: FCE with low soot particle abundance; right: FCE with high soot
1733 particle abundance. Trajectory end point: Schmäcke (10°46'15" E, 50°39'19" N, 500 m above
1734 model ground level). Temporal difference between successive trajectories: 2 hours.

1735

1736

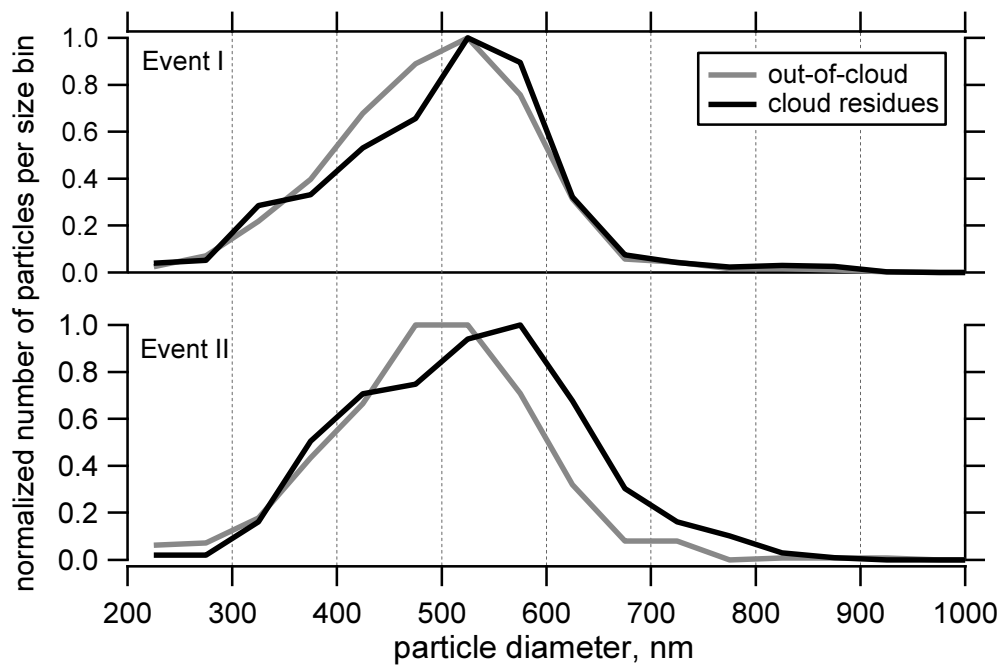
1737
1738



1739

1740 **Figure 11.** Indications for a change of particle mixing state in the cloud (for details of event I
1741 and II see Table 5). Left: Percentage of out-of-cloud aerosol particles and cloud residues
1742 containing either nitrate (blue) or sulphate (red). Right: Particles containing only nitrate but
1743 no sulphate (blue), only sulphate but no nitrate (red), and particles containing both nitrate and
1744 sulphate (purple).

1745
1746



1747

1748

1749 **Figure 12.** Histograms of particles analysed by ALABAMA during event I and event II
 1750 (Table 5). In both cases the histograms are shifted to larger sizes for the cloud residues,
 1751 indicating the uptake of gaseous compounds by the cloud droplets leading to an increased size
 1752 of the cloud residual particles compared to the out-of-cloud particles measured shortly before
 1753 cloud formation.